10926 *Inorg. Chem.* **2009**, *48*, 10926–10941
DOI: 10.1021/ic9010532

Inorganic Chemistry
Article

Characterization and Electronic Structures of Five Members of the Electron Transfer Series [Re(benzene-1,2-dithiolato)$_3$]^z (z = 1+, 0, 1−, 2−, 3−): A Spectroscopic and Density Functional Theoretical Study

Stephen Sproules,*,† Flávio Luiz Benedito,† Eckhard Bill,† Thomas Weyhermüller,† Serena DeBeer George,‡ and Karl Wieghardt*,†

†*Max-Planck-Institut für Bioanorganische Chemie, Stiftstrasse 34-36, D-45470 Mülheim an der Ruhr, Germany, and* ‡*Department of Chemistry and Chemical Biology, Baker Laboratory, Cornell University, Ithaca, New York 14853*

Received June 1, 2009

The reaction of $ReCl_5$ with 3 equiv of a benzene-1,2-dithiolate derivative in CH_3CN produced, after the addition of $[C_8H_{16}N]Br$ ($[C_8H_{16}N]^+$ is 5-azonia-spiro[4,4]nonane), brownish-green crystals of $[C_8H_{16}N][Re(tms)_3]$ (**1c**) and $[C_8H_{16}N][Re(Cl_2\text{-}bdt)_3]$ (**2c**), where $(tms)^{2-}$ represents 3,6-bis(trimethylsilyl)benzene-1,2-dithiolate and $(Cl_2\text{-}bdt)^{2-}$ is 3,6-dichlorobenzene-1,2-dithiolate. Chemical reduction of $[Re(bdt)_3]$ (**3b**) with *n*-butyllithium in the presence of PPh_4Br yielded $[PPh_4][Re(bdt)_3]$ (**3c**), where $(bdt)^{2-}$ is benzene-1,2-dithiolate. The three monoanionic complexes possess a diamagnetic ground state (Re(V), d^2, $S = 0$). The crystal structures of **1c**·$2CH_3CN$ and **2c**·C_3H_6O have been determined by X-ray crystallography. The electrochemistry establishes that the complexes are members of electron transfer series involving a monocation $[Re^V(L^\bullet)_2(L)]^+$ (S = 0(?)), a neutral $[Re^V(L^\bullet)(L)_2]^0$ ($S = {}^1/_2$), a monoanion $[Re^V(L)_3]^{1-}$ ($S = 0$), a dianion $[Re^{IV}(L)_3]^{2-}$ ($S = {}^1/_2$), and a trianion $[Re^{III}(L)_3]^{3-}$ (S = 1(?)). The unique X-band EPR spectrum of the neutral species clearly describes a diamagnetic Re(V) d^2 central ion with the unpaired electron located in a purely ligand-centered molecular orbital, whereas it is metal-centered in the dianionic form: a Re(IV) d^3 ion with three dithiolate(2−) ligands. S K-edge and Re L-edge X-ray absorption spectroscopy confirms these assignments and furthermore shows that the monoanion has a Re(V) central ion with three dianionic ligands. The geometrical and electronic structures of all members of the electron transfer series have been calculated by density functional theoretical methods, and the S K-pre-edge spectra have been simulated and assigned using a time-dependent DFT protocol.

Introduction

In their classic paper of 1966 Stiefel et al. reported[1] the synthesis and spectroscopic characterization in conjunction with electro- and magnetochemistry of three neutral tris-(dithiolene)rhenium complexes, namely, $[Re(pdt)_3]$,[2] $[Re(tdt)_3]$, and $[Re(bdt)_3]$, where the ligands are 1,2-diphenyl-1,2-dithiolate(2−), $(pdt)^{2-}$, and toluene-3,4-dithiolate-(2−), $(tdt)^{2-}$, and $(bdt)^{2-}$ is the unsubstituted benzene-1,2-dithiolate(2−). $[Re(pdt)_3]$ has been characterized by single crystal X-ray crystallography to be the first authenticated molecular example of a trigonal prismatic coordination compound in the solid state and solution.[3] At the time, these authors[1,4] showed that each of these neutral complexes is a member of an electron transfer series which involves a monocation; the above neutral species; and a mono-, a di-, and—at times—a trianion, eq 1.

$$\underset{S=0\,(?)}{[Re(L)_3]^+} \overset{E^1_{1/2}}{\underset{-e}{\rightleftharpoons}} \underset{S={}^1/_2}{[Re(L)_3]^0} \overset{E^2_{1/2}}{\underset{-e}{\rightleftharpoons}} \underset{S=0}{[Re(L)_3]^{1-}} \overset{E^3_{1/2}}{\underset{-e}{\rightleftharpoons}} \underset{S={}^1/_2}{[Re(L)_3]^{2-}} \overset{E^4_{1/2}}{\underset{-e}{\rightleftharpoons}} \underset{S=1\,(?)}{[Re(L)_3]^{3-}} \quad (1)$$

The neutral complexes possess an $S = {}^1/_2$ ground state, and their X-band electron paramagnetic resonance (EPR) spectra have been reported,[1,5] though controversially interpreted. Porte and Al-Mowali[5] have concluded from the observed **g** tensor anisotropy that a sulfur-centered radical $(L^\bullet)^-$ is present rather than a metal-centered paramagnet (Re(VI), d^1).

*To whom correspondence should be addressed. E-mail: sproules@mpi-muelheim.mpg.de (S.S.), wieghardt@mpi-muelheim.mpg.de (K.W.).

(1) Stiefel, E. I.; Eisenberg, R.; Rosenberg, R. C.; Gray, H. B. *J. Am. Chem. Soc.* **1966**, *88*, 2956.
(2) Schrauzer, G. N.; Mayweg, V. P. *J. Am. Chem. Soc.* **1966**, *88*, 3235.
(3) (a) Eisenberg, R.; Ibers, J. A. *J. Am. Chem. Soc.* **1965**, *87*, 3776. (b) Eisenberg, R.; Ibers, J. A. *Inorg. Chem.* **1966**, *5*, 411. (c) Eisenberg, R.; Brennessel, W. W. *Acta Crystallogr.* **2006**, *C62*, m464.
(4) Wharton, E. J.; McCleverty, J. A. *J. Chem. Soc. A* **1969**, 2258.
(5) Al-Mowali, A. H.; Porte, A. L. *J. Chem. Soc., Dalton Trans.* **1975**, 250.

 Published on Web 10/15/2009

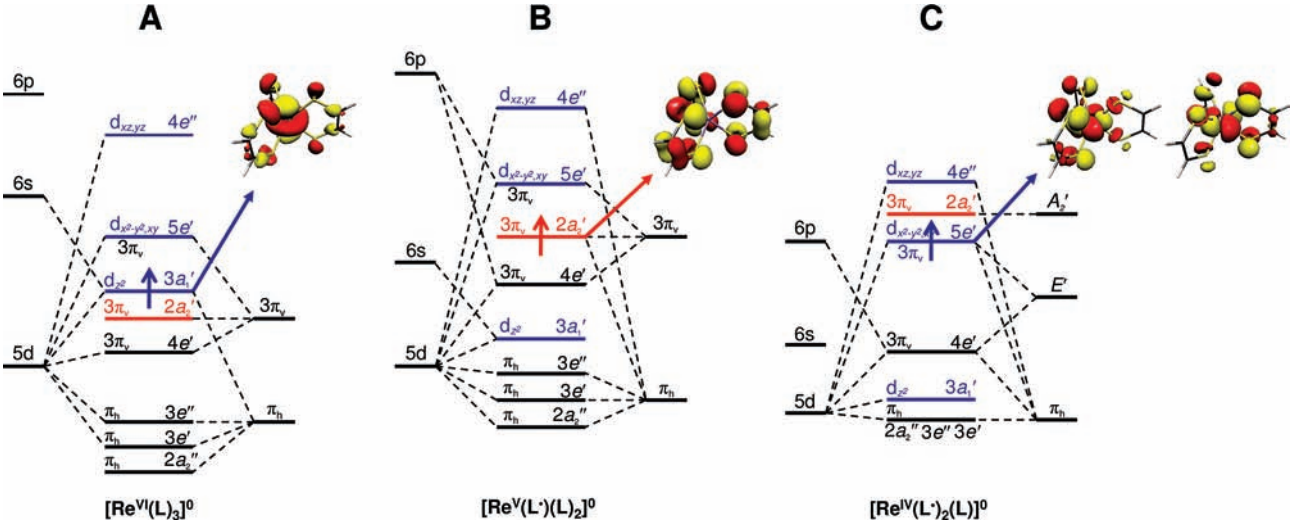

Figure 1. Qualitative MO schemes for trigonal prismatic $[Re(pdt)_3]^0$ as proposed by (A) Gray et al. in ref 1 with a $3a_1'$ SOMO (A), by Al-Mowali and Porte in ref 5 with a $2a_2'$ SOMO (B), and Schrauzer and Mayweg in ref 2 with a $5e'$ SOMO (C). Metal d orbitals are depicted in blue; $2a_2'$ MO in red.

Surprisingly few charged members of the above electron transfer series have been isolated, and none has been structurally characterized to date. Gray et al.[6] and McCleverty et al.[7] describe the paramagnetic ($S = {}^1/_2$) dianion in $[AsPh_4]_2[Re(mnt)_3]$ where $(mnt)^{2-}$ represents maleonitriledithiolate(2−). Despite its $S = {}^1/_2$ ground state, it did not provide an EPR spectrum at room temperature. Only one isolated monoanionic species has been reported in $[NEt_4][Re(Cl_4\text{-}bdt)_3]$, where $(Cl_4\text{-}bdt)^{2-}$ represents tetrachlorobenzene-1,2-dithiolate(2−).[4] The complex is diamagnetic; its structure is not known. No trianionic $[Re(L)_3]^{3-}$ species has been isolated to date. Therefore, with the notable exception of the neutral complexes,[1,2,5] the molecular and electronic structures of the electrochemical series comprising the monocationic and those of the mono-, di-, and trianionic species are not adequately described to date.

For the above neutral species, early calculations have resulted in three different proposals for the electronic structure of these trigonal prismatic compounds:

1. Gray et al.[1] proposed the molecular orbital (MO) scheme shown in Figure 1A where the unpaired electron resides in a predominantly metal-centered d_{z^2} orbital ($3a_1'$; ground state: $(4e')^4(2a_2')^2(3a_1')^1$), which can be depicted as trigonal prismatic $[Re^{VI}(L)_3]$ containing a central Re(VI) ion (d^1) and three closed-shell dianionic ligands.

2. Schrauzer and Mayweg,[2] on the other hand, concluded that $(3a_1')^2(4e')^4(5e')^1$ is the ground state (Figure 1C), which would encompass a filled d_{z^2} metal orbital and a half-filled $d_{x^2-y^2}/d_{xy}$ orbital (d^3 electron configuration) as in $[Re^{IV}(L^{\bullet})_2(L)]$.[8] Thus, the $(pdt)^{2-}$ ligands would show some degree of oxidation (two valence holes in the S 3p orbitals).

3. Finally, Al-Mowali and Porte[5] suggested, in 1975, the MO scheme shown in Figure 1B, where the unpaired electron resides in a ligand-centered orbital (ground state configuration $(3a_1')^2(4e')^4(2a_2')^1$). This may be described as $[Re^{V}(L^{\bullet})(L)_2]$ with a single valence hole in the ligands.[8] The central rhenium(V) ion possesses a diamagnetic ground state configuration $(d_{z^2})^2$; the unpaired electron resides in the $2a_2'$ orbital.

In order to resolve this question regarding the correct description of these neutral species experimentally, we have synthesized new monoanionic complexes containing the monoanion $[Re(tms)_3]^{1-}$ in **1c**, $[Re(Cl_2\text{-}bdt)_3]^{1-}$ in **2c**, and $[Re(bdt)_3]^{1-}$ in **3c**. The neutral complex **3b** has been prepared as described in ref 1. Scheme 1 shows the complexes, ligands, and their abbreviations, which are as follows: **a** = monocation, **b** = neutral, **c** = monoanion, **d** = dianion, and **e** = trianion.

We have measured the S K-edge X-ray absorption spectra (XAS) of these complexes and their corresponding analogues from the respective electron transfer series. This spectroscopy has been developed by the Solomon group[9] and has in recent years been successfully applied to detect π radical character in *S*,*S*′-coordinated dithiolene ligands.[10−15] We have also

(6) Stiefel, E. I.; Bennett, L. E.; Dori, Z.; Crawford, T. H.; Simo, C.; Gray, H. B. *Inorg. Chem.* **1970**, *9*, 281.
(7) Connelly, N. G.; Jones, C. J.; McCleverty, J. A. *J. Chem. Soc. A* **1971**, 712.
(8) It is most important to note that our use of the "L$^{\bullet}$" notation to represent a "ligand radical" or "ligand hole" is not meant to imply that the radical or hole is localized on one ligand. For analogous bis(dithiolene) complexes and octahedral complexes of Cr (ref 41), it is highly possible that the radical is localized, however, in a trigonal prismatic ligand field, the three dithiolene ligands together form one redox center, and that the radical or hole is shared equally amongst all three dithiolene ligands. Although the ligand system is better represented as $[(L)_3]^{5-}$, we continue to use our "L$^{\bullet}$" notation because it simplifies both electron counting and complex formulation.
(9) Glaser, T.; Hedman, B.; Hodgson, K. O.; Solomon, E. I. *Acc. Chem. Res.* **2000**, *33*, 859.
(10) (a) Sarangi, R.; DeBeer George, S.; Jackson Rudd, D.; Szilagyi, R. K.; Ribas, X.; Rovira, C.; Almeida, M.; Hodgson, K. O.; Hedman, B.; Solomon, E. I. *J. Am. Chem. Soc.* **2007**, *129*, 2316. (b) Szilagyi, R. K.; Lim, B. S.; Glaser, T.; Holm, R. H.; Hedman, B.; Hodgson, K. O.; Solomon, E. I. *J. Am. Chem. Soc.* **2003**, *125*, 9158.
(11) Tenderholt, A. L.; Szilagyi, R. K.; Holm, R. H.; Hodgson, K. O.; Hedman, B.; Solomon, E. I. *Inorg. Chem.* **2008**, *47*, 6382.
(12) Kapre, R. R.; Bothe, E.; Weyhermüller, T.; DeBeer George, S.; Muresan, N.; Wieghardt, K. *Inorg. Chem.* **2007**, *46*, 7827.
(13) Kapre, R. R.; Bothe, E.; Weyhermüller, T.; DeBeer George, S.; Wieghardt, K. *Inorg. Chem.* **2007**, *46*, 5642.
(14) (a) Kapre, R. R.; Ray, K.; Sylvestre, I.; Weyhermüller, T.; DeBeer George, S.; Neese, F.; Wieghardt, K. *Inorg. Chem.* **2006**, *45*, 3499. (b) Ray, K.; DeBeer George, S.; Solomon, E. I.; Wieghardt, K.; Neese, F. *Chem.—Eur. J.* **2007**, *13*, 2783.
(15) Pap, J. S.; Benedito, F. L.; Bothe, E.; Bill, E.; DeBeer George, S.; Weyhermüller, T.; Wieghardt, K. *Inorg. Chem.* **2007**, *46*, 4187.

Scheme 1. Ligands and Complexes

Ligands

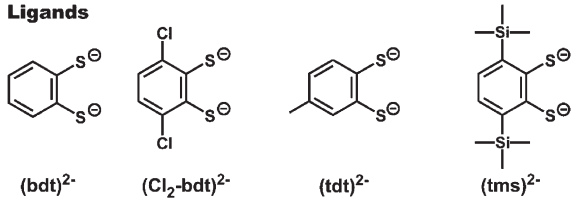

Complexes

$[C_8H_{16}N][Re(tms)_3]\cdot 2\,CH_3CN$	S = 0	**1c**
$[C_8H_{16}N][Re(Cl_2\text{-}bdt)_3]\cdot C_3H_6O$	S = 0	**2c**
$[Re(bdt)_3]^0$	S = 1/2	**3b**
$[PPh_4][Re(bdt)_3]$	S = 0	**3c**

measured and, for the first time, interpreted the X-band EPR spectra of the neutral and dianionic species, both with $S = {}^1/_2$ ground states. Finally, we have calculated the geometry and electronic structures of the five members of the electron transfer series and explored the stability of a trigonal prismatic structure over an octahedral one.

Experimental Section

Syntheses of Complexes. All air-sensitive materials were manipulated using standard Schlenk techniques or a glovebox. The neutral species $[Re(bdt)_3]$ (**3b**) has been prepared as described in ref 1, using chloroform in place of carbon tetrachloride, and the ligand 3,6-bis(trimethylsilyl)benzene-1,2-dithiol has been synthesized as described in ref 15. The salt 5-azonia-spiro[4,4]nonane bromide ($[C_8H_{16}N]Br$) was prepared according to the method of Schmidbaur et al.[16] The ligand 3,6-dichlorobenzene-1,2-dithiol was commercially obtained and used without further purification.

$[C_8H_{16}N][Re^V(tms)_3]\cdot 2CH_3CN$ (1c). The dipotassium salt, $K_2(tms)$, was produced by treating a suspension of 3,6-bis-(trimethylsilyl)benzene-1,2-dithiol (100 mg; 0.35 mmol) in 4 mL of dry acetonitrile with potassium *tert*-butoxide (KO^tBu; 76 mg; 0.68 mmol) and stirring (30 min) at ambient temperature. To the resulting yellow solution was added $ReCl_5$ (33 mg; 0.09 mmol) and $[C_8H_{16}N]Br$ ($(C_8H_{16}N)^+$ is 5-azonia-spiro-[4,4]nonane; 20 mg; 0.18 mmol). After stirring for 60 min at 20 °C, a brown solution was obtained which was filtered through Celite and exposed to the air. Brownish-green crystals of **1c** were grown from concentrated CH_3CN solutions. Yield: 57 mg (55%). Anal. Calcd for $C_{48}H_{82}N_3Si_6S_6Re$: C, 49.39; H, 7.03; N, 3.60. Found: C, 49.40; H, 7.06; N, 3.56.

$[C_8H_{16}N][Re^V(Cl_2\text{-}bdt)_3]\cdot C_3H_6O$ (2c). The complex was synthesized as described above for **1c** using 3,6-dichlorobenzene-1,2-dithiol as a starting material. Recrystallization of the crude product from acetone afforded crystals of **2c**. Yield: 80 mg (53%). Anal. Calcd for $C_{29}H_{28}NOS_6Cl_6Re$: C, 37.07; H, 2.98; N, 1.49. Found: C, 37.18; H, 2.87; N, 1.54.

$[PPh_4][Re^V(bdt)_3]$ (3c). To a tetrahydrofuran (10 mL) solution of $[Re(bdt)_3]$ (**3b**) (100 mg; 0.165 mmol) was added *n*-butyllithium (1.6 M in hexanes; 103 μL; 0.165 mmol) under anaerobic conditions (argon), and the solution was stirred for 10 min. The resulting dark brown solution was filtered and added to a solution of methanol (25 mL) containing $[PPh_4]Br$ (70 mg; 0.165 mmol). A brown crystalline precipitate formed which was collected by filtration, washed with methanol, and dried in vacuo. Yield: 114 mg (73%). Anal. Calcd for $C_{42}H_{32}PS_6Re$: C, 53.31; H, 3.41. Found: C, 52.71; H, 3.42.

Table 1. Crystallographic Data for **1c**·$2CH_3CN$ and **2c**·C_3H_6O

	1c·$2CH_3CN$	**2c**·C_3H_6O
chem. formula	$C_{48}H_{82}N_3Si_6S_6Re$	$C_{29}H_{28}NOS_6Cl_6Re$
fw	1248.27	997.78
space group	*Cmca*, No. 64	$P2_1/n$, No. 14
a, Å	17.6026(5)	12.9802(3)
b, Å	22.7323(5)	13.9055(3)
c, Å	31.6701(8)	20.4137(5)
β, deg	90	107.925(3)
V, Å	12672.7(6)	3505.74(14)
Z	8	4
T, K	100(2)	100(2)
ρ calcd, g cm^{-3}	1.309	1.890
reflns collected/$2\Theta_{max}$	80046/60.00	91435/65.00
unique reflns/$I > 2\sigma(I)$	9464/8441	12678/11018
No. of params/restr.	326/6	399/0
λ, Å/μ(Kα), cm^{-1}	0.71073/22.61	0.71073/43.09
R1[a]/goodness of fit[b]	0.0736/1.347	0.0294/1.041
wR2[c] ($I > 2\sigma(I)$)	0.1674	0.0647
residual density, eÅ^{-3}	+2.60/−5.60	+1.20/−2.17

[a] Observation criterion: $I > 2\sigma(I)$. $R1 = \sum||F_o| - |F_c||/\sum|F_o|$. [b] $GoF = [\sum w(F_o^2 - F_c^2)^2]/(n-p)]^{1/2}$. [c] $wR2 = [\sum[w(F_o^2 - F_c^2)^2]/\sum[w(F_o^2)^2]]^{1/2}$, where $w = 1/\sigma^2(F_o^2) + (aP)^2 + bP$, $P = (F_o^2 + 2F_c^2)/3$.

X-Ray Crystallographic Data Collection and Refinement of the Structures. Single crystals of compounds **1c**·$2CH_3CN$ and **2c**·C_3H_6O were coated with perfluoropolyether, picked up with nylon loops, and immediately mounted in the nitrogen cold stream of a Bruker-Nonius Kappa CCD diffractometer equipped with a Mo-target rotating-anode X-ray source (Mo Kα radiation, $\lambda = 0.71073$ Å) and a graphite monochromator. Final cell constants were obtained from least-squares fits of all measured reflections. Intensity data were corrected for absorption using intensities of redundant reflections with the program SADABS.[17] The structures were readily solved by Patterson methods and subsequent difference Fourier techniques. The Siemens ShelXTL[18] software package was used for solution and artwork of the structures; ShelXL97[19] was used for the refinement. All non-hydrogen atoms were anisotropically refined, and hydrogen atoms were placed at calculated positions and refined as riding atoms with isotropic displacement parameters. Crystallographic data of the compounds are listed in Table 1.

Several crystals and crystal fragments of **1c** were examined on the diffractometer. The best specimen was used for data collection, but the quality of the resulting data set was found to be quite low. This is due to an unresolved nonmerohedral twinning problem, which is further reflected in a high mosaicity, elevated standard deviations, moderate intensities of reflections which should be systematically absent, and an unusually high second weighting parameter. Careful attempts to refine the structure in lower symmetry space groups did not yield better results. Two acetonitrile solvent molecules are located on crystallographic mirror planes and are not well-defined. N−C and C−C distances were fixed with the DFIX instruction of ShelXL97.

X-Ray Absorption Spectroscopy. All data were measured at the Stanford Synchrotron Radiation Lightsource under ring conditions of 3.0 GeV and 60−100 mA. S K-edge data were measured using the 54-pole wiggler beamline 6-2 in a high-magnetic field mode of 10 kG with a Ni-coated harmonic rejection mirror and a fully tuned Si(111) double-crystal monochromator. Details of the optimization of this setup for low

(16) Schmidbaur, H.; Wohlleben, A.; Schubert, U.; Frank, A.; Huttner, G. *Chem. Ber.* **1977**, *110*, 145.

(17) Sheldrick, G. M. *SADABS*, version 2006/1; Universität Göttingen: Göttingen, Germany, 2006.

(18) *ShelXTL 6.14*; Bruker AXS Inc.: Madison, WI, 2003.

(19) Sheldrick, G. M. *ShelXL97*; Universität Göttingen: Göttingen, Germany, 1997.

energy have been previously described.[20] All samples were measured at room temperature as fluorescence spectra using a Lytle detector. Samples were ground finely and dispersed as thinly as possible on Mylar tape to minimize the possibility of fluorescence saturation effects or run in dichloromethane solutions of ~2 mM concentration. Data represent 2−3 scan averages. All samples were monitored for photoreduction throughout the course of data collection. The S K-edge energy was calibrated using the S K-edge spectra of $Na_2S_2O_3 \cdot 5H_2O$, run at intervals between sample scans. The maximum of the first pre-edge feature in the spectrum was fixed at 2472.02 eV. A step size of 0.08 eV was used over the edge region. Data were averaged, and a smooth background was removed from all spectra by fitting a polynomial to the pre-edge region and subtracting this polynomial from the entire spectrum. Normalization of the data was accomplished by fitting a flattened polynomial or straight line to the postedge region and normalizing the postedge to 1.0.

Re L-edge XAS data were measured using the focused 16-pole wiggler beamline 9-3. A Si(220) monochromator was utilized for energy selection, and a harmonic rejection mirror was present to minimize higher harmonic components in the X-ray beam. The solid samples were prepared as a dilute matrix in boron nitride, pressed into a pellet, and sealed between 38 μm Kapton tape windows in a 1 mm aluminum spacer. The sample of **3d** was prepared by controlled potential coulometry at −25 °C in a dichloromethane solution containing 0.10 M $[N(n\text{-}Bu)_4]PF_6$. Samples were maintained at 10 K during data collection by using an Oxford Instruments CF1208 continuous flow liquid helium cryostat. Data were measured in the transmission mode. Internal energy calibrations were performed by simultaneous measurement of the Re reference foil placed between a second and third ionization chamber with inflection points assigned as 12 527, 11 959, and 10 535 eV for the L_1-, L_2-, and L_3-edges, respectively. Data represent 2−4 scan averages and were processed by fitting a second-order polynomial to the pre-edge region and subtracting this background from the entire spectrum. A three-region cubic spline was used to model the smooth background above the edge. The data were normalized by subtracting the spline and normalizing the postedge to 1.0. Fits to the pre-edges modeled by pseudo-Voigt lines were carried out using the program EDG_FIT[21] with a fixed 1:1 ratio of Lorentzian to Gaussian contributions.

Other Physical Measurements. Cyclic voltammograms (CVs) and coulometric measurements were performed with an EG&G potentiostat/galvanostat. Electronic absorption spectra from the spectroelectrochemical measurements were obtained on a Hewlett-Packard 8453 diode-array spectrophotometer (range 200−1100 nm). X-band EPR spectra were recorded with a Bruker ESP 300 spectrometer. The spectra were simulated on the basis of a spin-Hamiltonian description of the electronic ground state with $S = {}^1/_2$:

$$\hat{H} = \mu_B \vec{B} \cdot g \cdot \hat{\vec{S}} + \hat{\vec{S}} \cdot A \cdot \hat{\vec{I}} + \hat{\vec{I}} \cdot P \cdot \hat{\vec{I}}$$

by using the simulation package XSOPHE.[22]

Calculations. All calculations in this work were performed with the electronic structure program ORCA.[23] Geometry optimizations were carried out using the B3LYP functional.[24] A segmented all-electron relativistically contracted basis set of triple-ζ-quality (TZVP) was used for rhenium.[25] A scalar relativistic correction was applied using the zeroth-order regular approximation (ZORA) method.[26] In the context of ZORA, a one-center approximation has been shown to introduce only minor errors to the final geometries.[26b] An all-electron polarized triple-ζ-quality (TZVP) basis set of Ahlrich's group was used for sulfur.[27] The remaining atoms were described by slightly smaller polarized split-valence SV(P) basis sets that are double-ζ-quality in the valence region and contain a polarizing set of d functions for the non-hydrogen atoms.[27c] Auxiliary basis sets for all complexes used to expand the electron density in the calculations were chosen to match the orbital basis. The self-consistent field calculations were tightly converged (1×10^{-8} E_h in energy, 1×10^{-7} E_h in the density change, and 1×10^{-7} in the maximum element of the DIIS[28] error vector). The geometry search for all complexes was carried out in redundant internal coordinates without imposing geometry constraints. The coordinates for the sequentially (~3.5°) twisted molecules for the $[Re(bdt)_3]^z$ ($z = 1+, 0, 1-, 2-$) were generated with the Z-matrix editor in Molden.[29] A broken symmetry BS(1,1) state was calculated for $[Re(bdt)_3]^+$ using the method of Noodleman and coworkers.[12,30] We adopted the following notation: The given system was divided into two fragments. The notation BS(m,n) refers then to a broken symmetry state with m unpaired α-spin electrons essentially on fragment 1 and n unpaired β-spin electrons localized on fragment 2. In most cases, fragments 1 and 2 correspond to the metal and the ligands, respectively. In this notation, the standard high-spin, open-shell solution is written as BS($m + n$,0). The BS(m,n) notation refers to the initial guess of the wave function. The variational process does, however, have the freedom to converge to a solution of the form BS($m - n$,0) in which effectively the n β-spin electrons pair up with $n < m$ α-spin electrons on the partner fragment. Such a solution is then a standard $M_S \cong (m - n)/2$ spin-unrestricted Kohn−Sham solution. As explained elsewhere,[31] the nature of the solution is investigated from the corresponding orbital transformation, which, from the corresponding orbital overlaps, displays whether the system should be described as a spin-coupled or a closed-shell solution. Single point energies were run using the same conditions detailed for the optimization. Canonical orbitals and density plots were constructed using the program Molekel.[32]

Time-dependent (TD-DFT) calculations of the sulfur K-pre-edges using the BP86 functional were conducted as previously described.[15,33] A single point, spin-unrestricted ground state DFT calculation, starting from the optimized coordinates and using the same basis sets described above, was performed.

(20) Hedman, B.; Frank, P.; Gheller, S. F.; Roe, A. L.; Newton, W. E.; Hodgson, K. O. *J. Am. Chem. Soc.* **1988**, *110*, 3798.
(21) George, G. N. *EXAFSPAK & EDG_FIT*; Stanford Synchrotron Radiation Lightsource, Stanford Linear Accelerator Center, Stanford University: Palo Alto, CA, 2000.
(22) Hanson, G. R.; Gates, K. E.; Noble, C. J.; Griffin, M.; Mitchell, A.; Benson, S. *J. Inorg. Biochem.* **2004**, *98*, 903.
(23) Neese, F. *Orca*, version 2.6, revision 35; Universität Bonn: Bonn, Germany, 2008.
(24) (a) Becke, A. D. *J. Chem. Phys.* **1993**, *98*, 5648. (b) Lee, C. T.; Yang, W. T.; Parr, R. G. *Phys. Rev. B* **1988**, *37*, 785.
(25) Pantazis, D. A.; Chen, X.-Y.; Landis, C. R.; Neese, F. *J. Chem. Theory Comput.* **2008**, *4*, 908.
(26) (a) van Lenthe, E.; Snijders, J. G.; Baerends, E. J. *J. Chem. Phys.* **1996**, *105*, 6505. (b) van Lenthe, E.; Faas, S.; Snijders, J. G. *Chem. Phys. Lett.* **2000**, *328*, 107. (c) van Lenthe, E.; van der Avoird, A.; Wormer, P. E. S. *J. Chem. Phys.* **1998**, *98*, 5648.
(27) (a) Ahlrichs, R.; May, K. *Phys. Chem. Chem. Phys.* **2000**, *2*, 943. (b) Schäfer, A.; Horn, H.; Ahlrichs, R. *J. Chem. Phys.* **1992**, *97*, 2571. (c) Schäfer, A.; Huber, C.; Ahlrichs, R. *J. Chem. Phys.* **1994**, *100*, 5829.
(28) (a) Pulay, P. *Chem. Phys. Lett.* **1980**, *73*, 393. (b) Pulay, P. *J. Comput. Chem.* **1992**, *3*, 556.
(29) Schaftenaar, G.; Noordik, J. H. *J. Comput.-Aided Mol. Des.* **2000**, *14*, 123.
(30) Noodleman, L.; Peng, C. Y.; Case, D. A.; Monesca, J. M. *Coord. Chem. Rev.* **1995**, *144*, 199.
(31) Neese, F. *J. Phys. Chem. Solids* **2004**, *65*, 781.
(32) *Molekel*, Advanced Interactive 3D-Graphics for Molecular Sciences, Swiss National Supercomputing Center. http://www.cscs.ch/molkel (accessed September 2009)
(33) DeBeer George, S.; Petrenko, T.; Neese, F. *Inorg. Chim. Acta* **2008**, *361*, 965.

The six sulfur 1s orbitals were localized using the Pipek−Mezey criteria,[34] and the TD-DFT equations were solved[35] individually for each sulfur atom, excluding all but excitations originating from the sulfur 1s orbital.[14,33,36] Since the absolute calculated transition energies show large errors due to the shortcomings in the treatment of relativity and DFT potentials in the core regions,[33,37] it was established that a constant shift of +61.45 eV is required for this regime of basis sets and applied to the transition energies. Plots were obtained using a line broadening of 0.8 eV.

Results and Discussion

a. Syntheses. The neutral complex $[Re(bdt)_3]$ (**3b**) has been obtained from the reaction of $ReCl_5$ with 3 equiv of the ligand benzene-1,2-dithiol in $CHCl_3$ solutions.[1] Correspondingly, the reaction of $ReCl_5$ with 3 equiv of the ligand dipotassium[3,6-bis(trimethylsilyl)benzene-1,2-dithiolate][15] in acetonitrile in the presence of potassium *tert*-butyloxide afforded, upon the addition of 5-azoniaspiro[4,4]nonane bromide, $[C_8H_{16}N]Br$,[16] brown-green crystals of $[C_8H_{16}N][Re(tms)_3]\cdot 2CH_3CN$ (**1c**). The complex $[C_8H_{16}N][Re(Cl_2\text{-}bdt)_3]\cdot C_3H_6O$ (**2c**) has been obtained in an analogous fashion using 3,6-dichlorobenzene-1,2-dithiol as a ligand. Reduction of the neutral complex **3b** with 1 equiv of *n*-butyllithium under anaerobic conditions in tetrahydrofuran solution yielded, upon addition of $[PPh_4]Br$, the complex $[PPh_4][Re(bdt)_3]$ (**3c**).

It has been established by ^1H NMR and temperature-dependent (3−300 K) magnetic susceptibility measurements[1] that the neutral complex **3b** possesses a paramagnetic $S = {}^1/_2$ ground state, whereas the monoanions in **1c**, **2c**, and **3c** are diamagnetic ($S = 0$). The dianion in **3d** possesses again an $S = {}^1/_2$ ground state. The spin ground states of the monocations $[Re(L)_3]^+$ and of the trianion $[Re(Cl_4\text{-}bdt)_3]^{3-}$[4] are not known, but−as shown below−the former is most likely diamagnetic ($S = 0$) whereas the latter is a $[Re^{III}(Cl_4\text{-}bdt)_3]^{3-}$ species with an $S = 1$ ground state.

b. Spectro- and Electrochemistry. Cyclic voltammograms of **1c**, **2c**, and **3b** have been recorded in CH_2Cl_2 solutions containing 0.10 M $[N(n\text{-}Bu)_4]PF_6$ at 25 °C. All potentials are referenced versus the ferrocenium/ferrocene (Fc^+/Fc) couple (ferrocene internal standard). The results are summarized in Table 2. Figure 2 displays the CV of **1c** and **3b**, where there are three and four reversible one-electron transfer waves observed, respectively, in the potential range +0.5 to −2.4 V. From coulometric measurements at fixed potentials, it has been established that the monoanion in **1c** is one-electron reduced at −1.9 V, affording a dianion but successively, twice one-electron oxidized at −0.30 V and +0.27 V, generating a neutral and then a monocationic species.

Similar results have been obtained for **2c**, where the second oxidation wave is not observed in the above potential range (Figure S1, Supporting Information). The CV of **3b** depicts the entire five-membered electron transfer series, where four reversible one-electron transfer processes are seen with $E_{1/2}{}^4$ occurring at very negative potentials (Figure 2). An effect of the aromatic ring substituent in complexes **1**, **2**, and **3** is clearly reflected in the redox potentials $E_{1/2}{}^2$, where the potential of the 0/1− couple increases in the order tms < bdt < Cl_2-bdt. Thus, electron-withdrawing chloro substituents in Cl_2-bdt ligands render its oxidation the most difficult process.

Table 2. Redox Potentials (V) of Complexes versus Fc^+/Fc

complex[a]	$E_{1/2}{}^1$ [b]	$E_{1/2}{}^2$ [c]	$E_{1/2}{}^3$ [d]	$E_{1/2}{}^4$ [e]
1c	+0.27	−0.30	−1.89	
2c		+0.45	−1.14	
3b	+0.43	−0.01	−1.43	−2.25
$[Re(Cl_4\text{-}bdt)_3]^{1-}$ [f]	+0.96	+0.33	−1.06	−1.73

[a] Recorded in CH_2Cl_2 solutions containing 0.1 M $[N(n\text{-}Bu)_4]PF_6$ at 25 °C using a scan rate of 100 mV s^{-1}. [b] 1+/0 couple. [c] 0/1− couple. [d] 1−/2− couple. [e] 2−/3− couple. [f] Ref 4. The original data recorded in CH_2Cl_2 were referenced versus an aqueous standard calomel electrode (SCE) with LiCl; here, they are converted by adding −0.38 V.

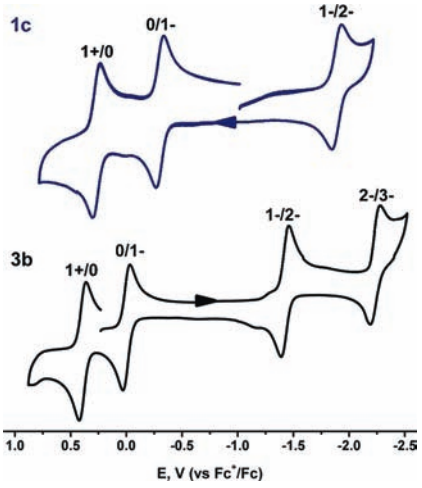

Figure 2. Cyclic voltammograms of **1c** and **3b** in CH_2Cl_2 solution (0.10 M $[N(n\text{-}Bu)_4]PF_6$ supporting electrolyte; 25 °C; scan rate, 100 mV s^{-1}; glassy carbon working electrode). Potentials are referenced versus Fc^+/Fc.

We have been able to generate electrochemically the monocation (**1a**), the neutral (**1b**), the monoanion (**1c**), and dianion (**1d**) forms of the series $[Re(tms)_3]^z$ and record their electronic spectra in a CH_2Cl_2 solution at −25 °C; they are shown in Figure 3 (top). The electrochemically generated species monoanion (**3c**) and dianion (**3d**) of **3b** are shown in Figure 3 (bottom). The oxidation of **3b** to a monocationic species (**3a**) is not reversible by controlled potential coulometry, as is the formation of the trianionic species, **3e**; hence, no electronic absorption spectra could be collected for these complexes. The data for all of the electrochemically isolated species are summarized in Table 3. Electrochemical oxidation of **2c** to form the neutral species, **2b** was incomplete, with only 16% of the desired product forming (Figure S2, Supporting Information). It is worthwhile to note that the electronic absorption spectra collected for each of the respective complex charges (1+, 0, 1−, 2−) are very similar, indicating that the electronic structure for each is independent of the ligand substitution.

The electronic spectra of the monocation and of the neutral species display an extremely intense ($\varepsilon > 10^4\ M^{-1}\ cm^{-1}$) charge transfer transition in the range 600−800 nm. This transition has been observed in previously

(34) Pipek, J.; Mezey, P. G. *J. Chem. Phys.* **1989**, *90*, 4916.
(35) Neese, F.; Olbrich, G. *Chem. Phys. Lett.* **2002**, *362*, 170.
(36) Milsmann, C.; Patra, G. K.; Bill, E.; Weyhermüller, T.; DeBeer George, S.; Wieghardt, K. *Inorg. Chem.* **2009**, *48*, 7430.
(37) DeBeer George, S.; Petrenko, T.; Neese, F. *J. Phys. Chem. A* **2008**, *112*, 12936.

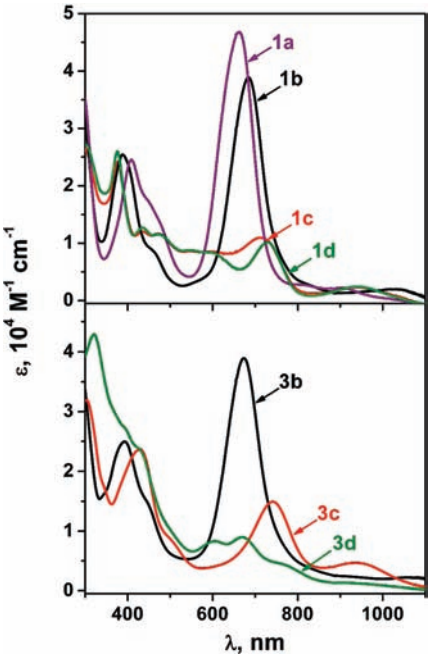

Figure 3. Electronic spectra of electrochemically generated monocation (purple), neutral molecules (black), monoanions (red), and dianions (green) of the series $[Re(tms)_3]^z$ ($z = 1+, 0, 1-, 2-$) (top) and the series $[Re(bdt)_3]^z$ ($z = 0, 1-, 2-$) (bottom) in CH_2Cl_2 (0.10 M $[N(n\text{-}Bu)_4]PF_6$) at −25 °C.

Table 3. Electronic Spectra of Electrochemically Generated Species in CH_2Cl_2 Solutions (0.10 M $[N(n\text{-}Bu)_4]PF_6$) at −25 °C

complex	λ_{max}, nm (ε, 10^4 M^{-1} cm^{-1})
1a	409(2.45), 454(1.67), 661(4.67), 811(0.27), 905(0.22)
1b	338(2.54), 459(sh, 0.87), 684(3.89), 841(0.23), 1026(0.19)
1c	376(2.54), 434(1.26), 437(1.15), 548(0.87), 599(0.85), 712(1.09), 941(0.24)
1d	377(2.42), 434(1.20), 473(1.15), 548(0.87), 599(0.85), 729(1.01), 941(0.21)
2c	313(5.90), 350(2.07), 411(2.22), 507(0.56), 730(1.81), 921(0.57)
2d	315(5.85), 360(3.30), 429(1.72), 603(0.73), 658(0.84), 737(0.38)
3b	390(2.50), 442(sh, 1.54), 674(3.89), 1062(0.22)
3c	304(3.19), 346(sh, 1.71), 429(2.36), 502(0.86), 742(1.49), 942(0.46)
3d	320(4.28), 393(sh, 2.73), 429(sh, 2.36), 605(0.83), 670(0.90), 765(0.44), 956(0.12)

reported neutral tris(dithiolene)molybdenum complexes,[1,2,13,38,39] which have recently been characterized as $[Mo^{V}(tbbdt^{\bullet})(tbbdt)_2]$ (tbbdt = 3,5-di-*tert*-butylbenzene-1,2-dithiolate)[13] or $[Mo^{IV}(mdt^{\bullet})_2(mdt)]$ (mdt = 1,2-dimethyl-1,2-dithiolate) species.[11] This band has been identified as a marker for the presence of an oxidized dithiolene ligand(s). From the DFT-derived qualitative MO scheme presented in Figure 12 (vide infra), we tentatively classify this as the $4e' \rightarrow 2a_2'$ transition since it has ∼90% ligand-to-ligand charge transfer (LLCT) character with only a small amount of metal-to-ligand charge transfer (MLCT) character resulting from ∼8% Re $5d_{x^2-y^2,xy}$ contribution to the $4e'$ orbitals.

This band is absent in the spectra of the mono- and dianionic forms, $[Re^{V}(L)_3]^{1-}$ and $[Re^{IV}(L)_3]^{2-}$. This feature indicates the presence of three closed-shell dithiolate dianions and a rhenium(V) and rhenium(IV) central metal ion, respectively. The final member of these electron transfer series, $[Re^{III}(bdt)_3]^{3-}$ (**3e**), is generated at very negative potentials (−2.25 V) and is only reversible at −25 °C on the CV time scale. Similarly, the trianions $[Re(tdt)_3]^{3-}$ (tdt^{2-} = toluene-3,4-dithiolate) and $[Re(Cl_4\text{-}bdt)_3]^{3-}$ are also only observed electrochemically,[1,4] at potentials of −2.34 V[40] and −1.73 V versus Fc^+/Fc, respectively. No other spectroscopic data are available, but DFT calculations (see below) suggest a $[Re^{III}(bdt)_3]^{3-}$ electronic structure with a central Re(III) ion (d^4, $S = 1$) and three closed-shell dithiolate(2−) anions.

c. Crystal Structures of 1c and 2c. The crystal structures of **1c** and **2c** have been determined by X-ray crystallography. Both species consist of well-separated $[C_8H_{16}N]^+$ cations and $[Re(tms)_3]^{1-}$ and $[Re(Cl_2\text{-}bdt)_3]^{1-}$ monoanions, respectively. Figure 4 exhibits the structures of the monoanions in **1c** and **2c**. Table 4 summarizes selected bond distances.

The structure of *neutral* $[Re(pdt)_3]$ is also trigonal prismatic ($\Theta = 3.8°$), and Gray et al.[1] have suggested that $[Re(bdt)_3]$ (**3b**) has a similar structure. From our previous investigation[12,41] of $[Cr(L)_3]^{3-}$, containing an octahedral CrS_6 moiety with a central Cr(III) ion (d^3, $S = {}^3/_2$) and three closed-shell dithiolato(2−) anions, we propose that $[Re(bdt)_3]^{3-}$ also contains a distorted octahedral ReS_6 polyhedron with a central Re(III) ion (d^4, $S = 1$) and three closed-shell bdt^{2-} ligands. No structural data are available for dianionic $[Re(bdt)_3]^{2-}$ species, but a recent X-ray crystal structure determination of $[PPh_4]_2[Re(mnt)_3]$ ($S = {}^1/_2$; mnt^{2-} = maleonitriledithiolate) revealed a structure intermediate between a trigonal prism and an octahedron ($\Theta = 38.3°$).[42] The average fold angle is again very small.

d. Electron Paramagnetic Resonance (EPR) Spectroscopy. Neutral tris(dithiolene)rhenium complexes having a $S = {}^1/_2$ ground state have been analyzed by EPR spectroscopy and proved to be the key evidence that motivated Al-Mowali and Porte[5] to revise the published orbital manifolds of Gray et al.[1] and Schrauzer and Mayweg.[2] Gray et al.'s and Schrauzer and Mayweg's electronic structures depicted a Re(VI) d^1 and Re(IV) d^3 ion, respectively (Figure 1), placing the unpaired spin on the metal. Porte and Al-Mowali keenly observed that the frozen solution spectrum of $[Re(tdt)_3]$ was drastically different to that of $[ReOCl_4]$,[43] containing a Re(VI) central ion.[5] The EPR spectrum of the latter is characterized by a pronounced g anisotropy resulting from the large spin orbit coupling of the third row transition metal. Additionally, there is an even larger magnetic hyperfine interaction from the ^{185}Re (37.4% natural abundance) and ^{187}Re (62.6% natural abundance) nuclei that are both $I = {}^5/_2$, affording a spectrum that spans 500 mT, as typified by Re(VI)-nitrido species investigated by Abram and co-workers.[44]

(38) Formitchev, D.; Lim, B. S.; Holm, R. H. *Inorg. Chem.* **2001**, *40*, 645.
(39) Lim, B. S.; Donahue, J.; Holm, R. H. *Inorg. Chem.* **2000**, *39*, 263.
(40) The potential was determined in *N*,*N*′-dimethylformamide and referenced to Ag/AgCl. We arrived at an empirical conversion factor of −0.03 V to convert this potential to our scale.
(41) Banerjee, P.; Sproules, S.; Weyhermüller, T.; DeBeer George, S.; Wieghardt, K. *Inorg. Chem.* **2009**, *48*, 5829.
(42) Sproules, S.; Weyhermüller, T.; Wieghardt, K. Unpublished results.
(43) Al-Mowali, A. H.; Porte, A. L. *J. Chem. Soc., Dalton Trans.* **1975**, 50.
(44) (a) Abram, U.; Braun, M.; Abram, S.; Kirmse, R.; Voigt, A. *J. Chem. Soc., Dalton Trans.* **1998**, 231. (b) Abram, U.; Hagenbach, A.; Voigt, A.; Kirmse, R. *Z. Anorg. Allg. Chem.* **2001**, *627*, 955. (c) Abram, U.; Schmidt-Brücken, B.; Hagenbach, A.; Hecht, M.; Kirmse, R.; Voigt, A. *Z. Anorg. Allg. Chem.* **2003**, *629*, 838.

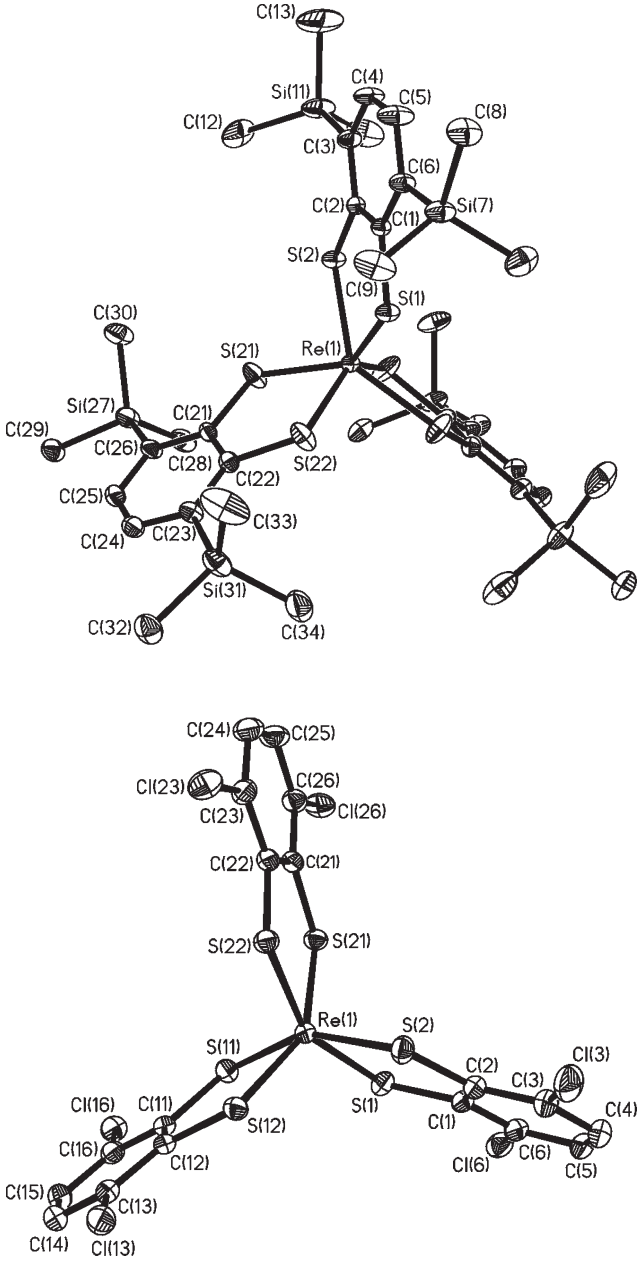

Figure 4. Structure of the monoanions in **1c** (top) and **2c** (bottom).

In contrast, $[Re(tdt)_3]$ has a narrow signal spanning only 15 mT, and a $(3a_1')^2(4e')^4(2a_2')^1$ electronic configuration was proposed with the unpaired electron located in a pure ligand orbital. While this is the correct electronic structure, as reiterated by our DFT calculations, Porte provided an erroneous simulation of the experimental spectrum. We have discovered that this complicated X-band spectrum results from a strong quadrupole interaction derived from a very large valence contribution to the electric field gradient (EFG) in conjunction with the sizable ^{185,187}Re nuclear quadrupole moments (2.8 and 2.6 $\times$ 10^{-24} cm^2, respectively).

The frozen glass spectra of **1b**, **2b**, and **3b** displayed in Figure 5 are almost indistinguishable. The simulation parameters are listed in Table 5, and given their similarity, one simulation is shown (in red, top) in Figure 5. They are identical to the published spectrum of $[Re(tdt)_3]$, with a

Table 4. Selected Bond Distances (Å) in **1c** and **2c**

	1c	2c
Re(1)−S(1)	2.341(2)	2.3513(6)
Re(1)−S(2)	2.358(2)	2.3373(6)
Re(1)−S(3)	2.330(2)	2.3279(6)
Re(1)−S(4)	2.345(2)	2.3390(6)
Re(1)−S(5)	2.330(2)	2.3371(6)
Re(1)−S(6)	2.345(2)	2.3476(6)
S(1)−C(1)	1.762(9)	1.745(3)
S(2)−C(2)	1.739(1)	1.737(3)
S(3)−C(7)	1.742(7)	1.738(2)
S(4)−C(12)	1.743(7)	1.740(2)
S(5)−C(13)	1.742(7)	1.740(2)
S(6)−C(18)	1.743(7)	1.735(2)
C(1)−C(2)	1.398(1)	1.400(4)
C(2)−C(3)	1.434(1)	1.407(4)
C(3)−C(4)	1.387(1)	1.382(4)
C(4)−C(5)	1.430(1)	1.387(5)
C(5)−C(6)	1.384(1)	1.381(4)
C(6)−C(1)	1.429(1)	1.403(4)
C(7)−C(8)	1.398(9)	1.401(3)
C(8)−C(9)	1.426(1)	1.406(3)
C(9)−C(10)	1.386(1)	1.377(4)
C(10)−C(11)	1.381(1)	1.394(4)
C(11)−C(12)	1.391(1)	1.381(4)
C(12)−C(7)	1.414(1)	1.402(3)
C(13)−C(14)	1.398(1)	1.401(3)
C14−C(15)	1.426(1)	1.406(3)
C(15)−C(16)	1.386(1)	1.377(4)
C(16)−C(17)	1.381(1)	1.394(4)
C(17)−C(18)	1.391(1)	1.381(4)
C18−C(13)	1.414(9)	1.402(3)

central signal at $g \sim 2.013$ flanked on either side by two features that were incorrectly assigned as **g** tensor components.[5] Importantly, the lower field feature exhibits a crossing point such that it cannot arise from the **g** tensor alone.[45] In fact, these signals stem from the combination of a small Re superhyperfine coupling of ~63 MHz with a very large quadrupole interaction, P = 73 MHz, where $P = [P_{zz} - (P_{xx} + P_{yy})/2]/3$. Nuclear quadrupole interactions can result in perturbations of the intensity and spacing of the $\Delta m_I = 0$ transitions.[46,47] Such an effect is operative here, with the expected "six-line" magnetic hyperfine interaction (given the isotropic **g** tensor) comprising $\Delta m_I = 0$ transitions that are compressed into the two flanking features of the central resonance. Additionally, we find a small pair of satellite signals 15 mT away from the central resonance (inset, Figure 5) that are quadrupole-allowed transitions traditionally not observed in EPR spectra. These are assigned

(45) The central line and its nearest satellites cannot be mistaken as the derivatives of an anisotropic powder spectrum with three separate **g** values because the corresponding absorption spectrum (the first integral), being a broad powder distribution, would have a unique maximum and two distinct shoulders. That pattern could exhibit only one unique zero crossing point in the derivative spectrum (at g_2), whereas the experimental traces show two crossing points at 335 and 330 mT (and a third on the right of the center is blurred by line broadening; see simulation). Furthermore, the low intensities of the satellites also do not fit to a powder distribution. Moreover, the remote satellites were not included in the published spectrum by Al-Mowali and Porte (ref 5).

(46) (a) Liczwek, D. L.; Belford, R. L.; Pilbrow, J. R.; Hyde, J. S. *J. Phys. Chem.* **1983**, *87*, 2509. (b) Connelly, N. G.; Emslie, D. J. H.; Klangsinsirikul, P.; Rieger, P. H. *J. Phys. Chem. A* **2002**, *106*, 12214. (c) Shaw, J. L.; Wolowska, J.; Collison, D.; Howard, J. A. K.; McInnes, E. J. L.; McMaster, J.; Blake, A. J.; Wilson, C.; Schröder, M. *J. Am. Chem. Soc.* **2006**, *128*, 13827.

(47) Huang, D.; Zhang, X.; McInnes, E. J. L.; McMaster, J.; Blake, A. J.; Davies, E. S.; Wolowska, J.; Wilson, C.; Schröder, M. *Inorg. Chem.* **2008**, *47*, 9919.

Scheme 2. Twist Angle Θ and Ligand Fold Angles α, α′, and α″

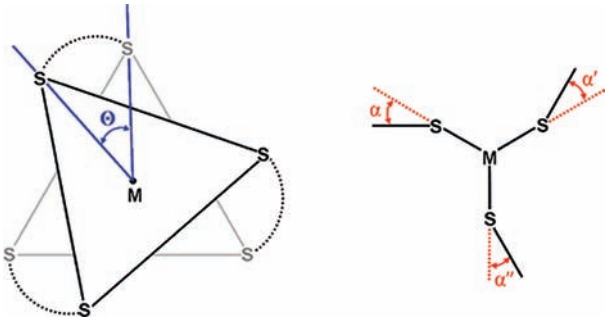

as the $\pm^1/_2 \rightarrow \pm^3/_2$ ($\Delta m_I = 1$) transitions since these have the smallest energy separation at 438 MHz (6*P*). *This very unique situation where the quadrupole interaction is larger than the magnetic hyperfine interaction can only arise if the spin is located on the ligand and the diamagnetic Re ion has a* $(d_{z^2})^2$ *electronic configuration.* This generates the very large valence contribution to the EFG producing the observable quadrupole-allowed transitions in the spectrum. Large quadrupole couplings that exceed the magnetic hyperfine interaction have only been observed for neutral square planar bis(dithiolene)gold(III).[48] Therefore, we can definitively affirm the electronic structure of these neutral tris(dithiolene)rhenium complexes as $[Re^V(L^\bullet)(L)_2]^0$.[8]

The doubly reduced dianionic species also has a $S = {}^1/_2$ ground state; however, there is no recorded EPR spectrum for such a complex. McCleverty et al. commented that $[PPh_4]_2[Re(mnt)_3]$ (mnt = maleonitriledithiolate) did not yield a signal at room temperature.[49] The EPR spectrum of **3d** at 20 K is shown in Figure 6 and is distinctly different from the spectra of the neutral species described above. The spectrum spans 450 mT, akin to the Re(VI) d^1 complexes of Abram et al.,[44] and clearly depicts a metal-centered paramagnet.

A very concentrated sample (~5 mM) was generated by controlled potential coulometry. A reasonably large modulation amplitude (1.5 mT) and high power (6.3 mW) were necessary to record the spectrum of **3d** at 20 K. The spectrum is characterized by six broad hyperfine lines, stemming from the magnetic hyperfine interaction of the ^{185,187}Re $I = {}^5/_2$ nuclei. There is a sharp signal at $g = 2.003$ that results from a small organic impurity, possibly from the solvent stabilizers, that accounts for <1% of the total absorption. Quadrupole effects produce the characteristic uneven splitting of the six hyperfine lines, and quadrupole-allowed transitions are seen in the low-field portion of the spectrum. These features have only been sparingly observed at X-band frequencies previously.[46] The simulation parameters for **3d** listed in Table 5 show rhombic **g** and **A** tensors, and an axial $P = (20, 20, -40) \times 10^{-4}$ cm^{-1} that gives a quadrupole coupling value of $P = 60$ MHz. It is important to note that the **A** tensor is rotated away from the **P** tensor (Euler angles: $\chi = 82°$; $\varsigma = 25°$; $\tau = -90°$); the **g** and **P** tensors are

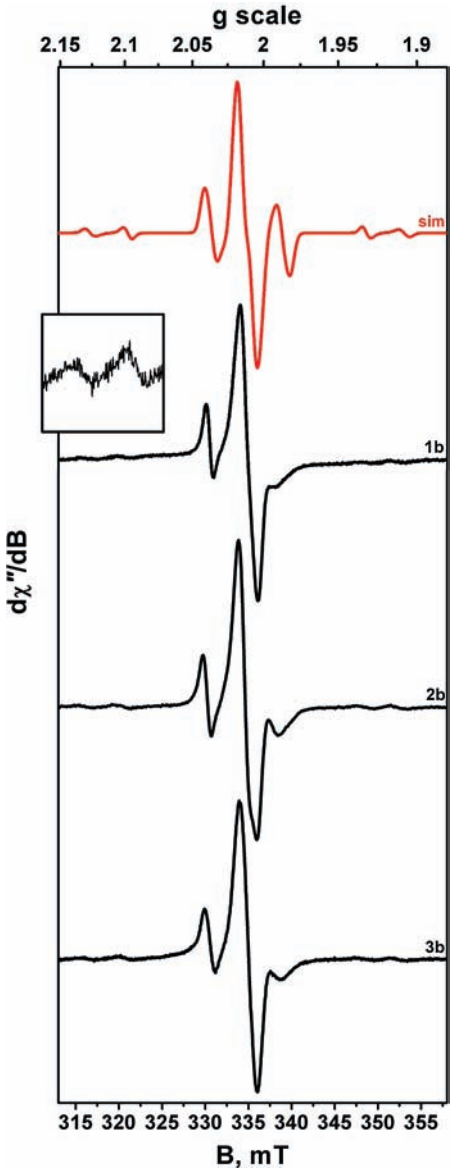

Figure 5. X-band EPR spectra of neutral $S = {}^1/_2$ complexes **1b**, **2b**, and **3b**. A representative simulation is shown in red (top), and parameters are given in the text and Table 5. Experimental spectra (black) in descending order: **1b** in CH_2Cl_2 at 10 K (conditions: frequency, 9.45 GHz; power, 0.2 mW; modulation, 0.7 mT); **2b** in CH_2Cl_2 at 30 K (conditions: frequency, 9.45 GHz; power, 0.01 mW; modulation, 1.0 mT); and **3b** in THF at 77 K (conditions: frequency, 9.24 GHz; power, 1.0 mW; modulation, 1.0 mT). The inset shows magnification of the satellite features found in each spectrum due to the large quadrupole interaction inherent to this electronic configuration.

Table 5. EPR Spin Hamiltonian **g** Tensor, Re Magnetic Hyperfine Tensor ($A \times 10^{-4}$ cm^{-1}),[a] and Re Electric Quadrupole Tensor ($P \times 10^{-4}$ cm^{-1}),[b] Derived from Simulation of the Neutral $S = {}^1/_2$ Complexes

	g_{xx}	g_{yy}	g_{zz}	A_{xx}	A_{yy}	A_{zz}	P_{xx}	P_{yy}	P_{zz}
1b	2.016	2.015	2.014	−31.0	−27.0	−4.0	24.2	24.2	−48.4
2b	2.015	2.015	2.015	−32.0	−25.0	−6.0	24.2	24.2	−48.4
3b	2.014	2.012	2.012	−29.0	−30.0	−4.5	24.3	24.3	−48.6
3d[c]	1.701	1.680	1.515	−310	−690	−100	20.0	20.0	−40.0

[a] The sign of the **A** tensor components is not unique and is assigned as negative assuming a dominating Fermi-contact contribution. [b] The sign of the **P** tensor components is not known from the simulation, so we assume the negative component to be the *z* direction. [c] **A** is rotated with respect to **P**, with angles $\chi = 82°$, $\zeta = 25°$, and $\tau = -90°$.

(48) Kokatam, S.; Ray, K.; Pap, J.; Bill, E.; Geiger, W. E.; LeSuer, R. J.; Rieger, P. H.; Weyhermüller, T.; Neese, F.; Wieghardt, K. *Inorg. Chem.* **2007**, *46*, 1100.

(49) McCleverty, J. A.; Locke, J.; Wharton, E. J.; Gerloch, M. *J. Chem. Soc. A* **1968**, 816.

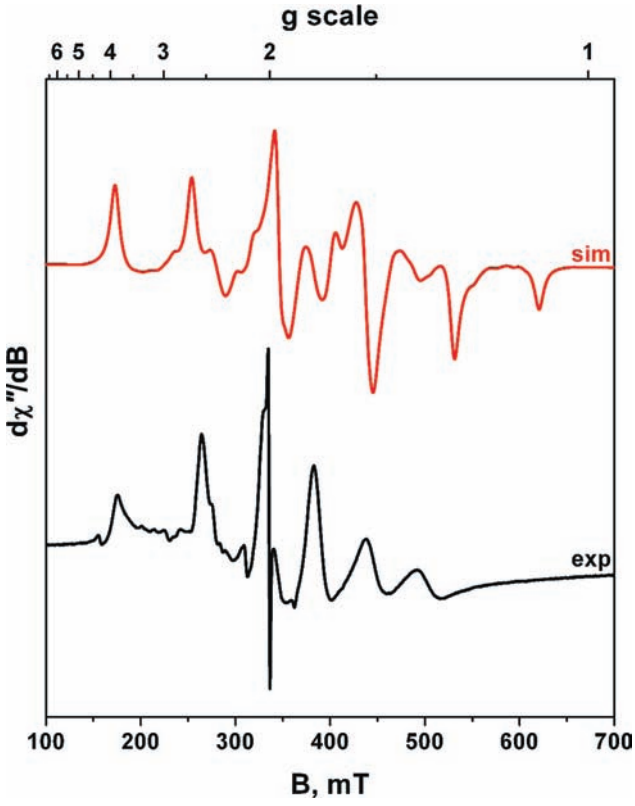

Figure 6. X-band EPR spectrum of **3d** in CH_2Cl_2 at 20 K. The simulation is shown in red with the experimental spectrum in black (conditions: frequency, 9.41 GHz; power, 6.3 mW; modulation, 1.5 mT).

coaxial. We have been unable to reproduce a number of the small quadrupole-allowed transitions at low field in the experiment spectrum, and these could result from a Gaussian distribution of the magnetic hyperfine with respect to the **P** tensor, such that we would need to perform single-crystal measurements to resolve such a complicated tensor orientation. However, it is clear from this spectrum that we can unambiguously assign a $[Re^{IV}(L)_3]^{2-}$ electronic structure to dianionic tris-(dithiolene)rhenium complexes, where the Re(IV) ion possesses a $(d_{z^2})^2(d_{x^2-y^2,xy})^1$ electron configuration, with the unpaired spin centered on the Re atom.

e. X-Ray Absorption Spectroscopy (XAS). i. Re L-Edge XAS. The Re L_1-edge spectra for **3b**, **3c**, and **3d**, where the latter was prepared electrochemically at −25 °C in dichloromethane solutions containing 0.10 M $[N(n\text{-}Bu)_4]PF_6$, are presented in Figure 7. We have measured at this edge since it is dominated by the Re 2s → 6p dipole-allowed transition; it roughly gives the same information as the K-edge because it measures the density of projected p states. Also, the pre-edge is sensitive to local geometry where dipole-forbidden 2s → 5d transitions gain intensity through 5d/6p mixing that is maximized in systems with noninversion centers.[50] For six-coordinate complexes, d−p hybridization occurs most strongly in trigonal prismatic geometry, while it is absent in octahedral symmetry. The spectra shown in Figure 7 show a clear 1 eV difference in the rising edge energy for **3d** compared with **3b** and **3c**. This clearly demonstrates that a Re(IV) ion

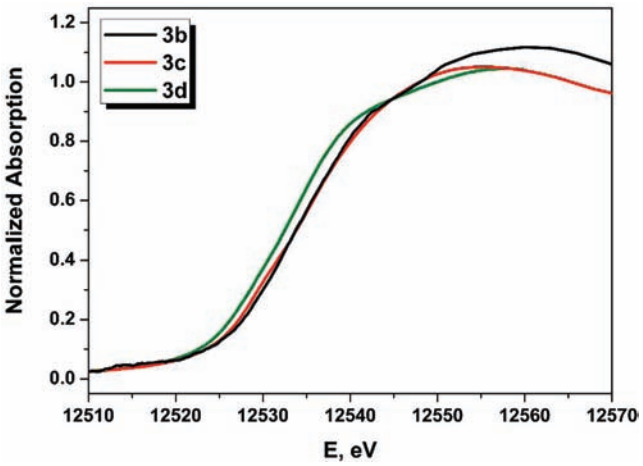

Figure 7. Normalized Re L_1-edge XAS data of $[Re(bdt)_3]$ (black), $[Re(bdt)_3]^{1-}$ (red), and $[Re(bdt)_3]^{2-}$ (green) in **3b**, **3c**, and **3d**.

exists in **3d** while the monoanion and neutral species possess a Re(V) center, in line with the outcome from the EPR measurements.

We find pre-edge region featureless despite the presumed trigonal prismatic geometry of **3b**. Pre-edge features have been observe at the Re L_1-edge for tetrahedral rhenium oxides,[51] which are apparently larger than the symmetry-derived 5d−6p hybrization in our system (DFT calculations estimate a 5.4% Re 6p mixing into the $5e'$ orbitals). We have observed an intense pre-edge due to significant 4p mixing into 3d orbitals in V K-edge spectra[52] and calculated Cr K-pre-edge spectra[41] where the pre-edge and near-edge regions of the spectrum are well-resolved, owing to the short core-hole lifetime for first row transition metals.

The Re L_3- and L_2-edge spectra for **1c**, **2c**, **3b**, **3c**, and **3d** are overlaid in Figure 8 and Figure S3 (Supporting Information), respectively, and contrast the absorption at the L_1-edge. Re $L_{3,2}$-edges result from the dipole-allowed 2p → 5d transitions, where spin−orbit coupling of the 2p hole generates $^2P_{3/2}$ (L_3-edge) and $^2P_{1/2}$ (L_2-edge) states, separated by ∼1424 eV. The energy of these transitions depends on the electronic structure of the metal site, and changes in the oxidation state, coordination number, and geometry will affect the energy of both the 2p and 5d orbitals. However, the 2p and 5d spin−orbit and the 2p core-hole−5d multiplet interactions may affect the intensities and energy distributions of these transitions and must be considered in any analysis of these edges.[53] Each compound exhibits a single intense absorption peak (white line); the transition energies are presented in Table 6. In both edges, the data display no obvious trend that reflects a different metal oxidation state, instead showing a ligand field splitting dominance of the edge energy.

In the Mo L_3-edge XAS spectra of analogous molybdenum compounds,[13] two peaks are observed, where the difference in the peak energy can be used to estimate the crystal field splitting and, hence, the coordination

(50) Shulman, R. G.; Yafet, Y.; Eisenberger, P.; Blumberg, W. E. *Proc. Natl. Acad. Sci. U. S. A.* **1976**, *73*, 1384.

(51) Lytle, F. W.; Greegor, R. B. *Appl. Phys. Lett.* **1990**, *56*, 192.

(52) Sproules, S.; Bill, E.; Weyhermüller, T.; DeBeer George, S.; Wieghardt, K. Manuscript in preparation.

(53) de Groot, F. M. F.; Hu, Z. W.; Lopez, M. F.; Kaindl, G.; Guillot, F.; Trone, M. *J. Chem. Phys.* **1994**, *101*, 6570.

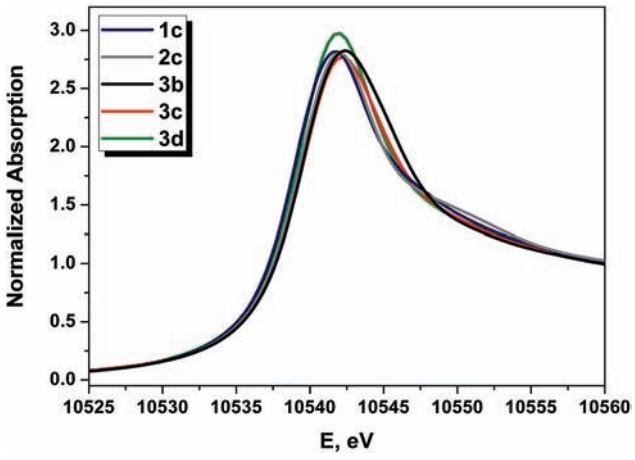

Figure 8. Normalized Re L_3-edge XAS data of $[Re(tms)_3]^{1-}$ (**1c**), $[Re(Cl_2\text{-}bdt)_3]^{1-}$ (**2c**), $[Re(bdt)_3]$ (**3b**), $[Re(bdt)_3]^{1-}$ (**3c**), and $[Re(bdt)_3]^{2-}$ (**3d**).

Table 6. Experimental Re L-Edge Transition Energies (eV) for the Complexes

	Re L-edge		
	L_3[a]	L_2[a]	L_1[b]
1c	10541.8	11964.5	nm[c]
2c	10541.8	11964.9	nm
3b	10542.1	11966.2	12533.6
3c	10541.9	11965.6	12533.9
3d	10541.6	11965.1	12532.6

[a] Transition energies determined from peak maxima. [b] Transition energy determined from the mid point of the rising edge. [c] nm = not measured.

geometry. This feature has been utilized in previous studies at the Re L_3-edge on rhenium-oxide-containing materials,[54] where two closely spaced maxima are observed for a Re ion in (distorted) tetrahedral or octahedral geometry. Here, linewidths of ~5 eV highlight the similar ligand field splitting for these complexes calculated to be trigonal prismatic (**1c** and **3b**) and distorted trigonal prismatic (**2c**, **3c**, and **3d**). The ligand field splitting is too small to be observed experimentally, which is a consequence of the longer core-hole lifetime for Re L-edges compared with Mo L-edges. The Re L_2-edge XAS spectra are also characterized by a single peak, and here again the peak energies do not present any trend that can be correlated with the effective nuclear charge alone.

ii. S K-edge XAS. Figure 9 displays the S K-edge X-ray absorption spectra of two members of the electron transfer series $[Re(tms)_3]^{0,1-}$ (**1b**, **1c**) recorded in dichloromethane solutions at room temperature. The neutral complex **1b** was prepared via in situ oxidation of **1c** by molecular iodine.

Both the neutral **1b** and monoanionic **1c** species have a resolved pre-edge feature at ~2471.0 eV. The spectrum of **1b** exhibits an additional lower energy pre-edge peak at 2470.05 eV. It has been established[11,13] that this transition is consistent with an extra hole in the dithiolene ligands

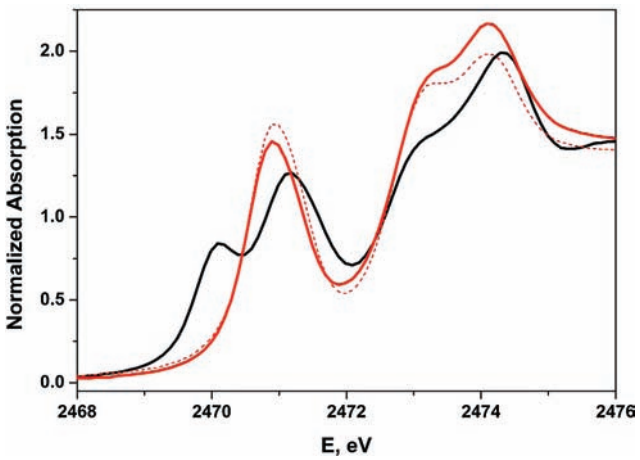

Figure 9. Comparison of the normalized S K-edge spectra of **1b** (black) and **1c** (red), recorded at room temperature in dichloromethane solutions. The dashed line is the spectrum of solid **1c**.

due to $1e^-$ oxidation, and it has been assigned here as a transition to the $2a_2'$ and confirms the assignment of a one-electron ligand oxidation of the monoanion generating the neutral species. The peaks at higher energy (> 2472 eV) are transitions to C−S π^* and C−S σ^* orbitals frequently observed in the spectra of dithiolene[10,12,13,41] and thiolate[55] complexes and are best assigned as "rising" edge features because they are followed by transitions to the sulfur 4p levels and finally into the continuum. The shift in the rising edge (comparing the peak at ~2474 eV in each spectrum) of ~0.25 eV to lower energy for **1c** compared to **1b** indicates more oxidized sulfur in the latter complex. The S K-edge spectrum of solid **1c** is overlaid with the solution spectrum in Figure 9 and shows the same peak energies. It is difficult to speculate whether the geometry is retained in solution since the difference in the total energy of these structures, at least in the gas phase, is miniscule (vide infra). However, the small increase in the pre-edge peak intensity could reflect a slight structural rearrangement in solution.

The S K-edge XAS spectra of **2c**, **3b**, and **3c** are presented in Figure S4 (Supporting Information). While their peak energies are consistent with the formulation discussed above, there are noticeable intensity differences when compared with **1b** and **1c** due to decomposition in the beam that precludes their inclusion in a quantitative analysis. The coulometrically generated sample of **3d** was not amenable to measurement at room temperature.

g. Calculations. In this section, a picture of the electronic structures of $[Re(tms)_3]^{+,0,1-,2-,3-}$ (**3a**, **3b**, **3c**, **3d**, and **3e**) as well as for $[Re(tms)_3]^{1-}$ (**1b**), $[Re(tms)_3]^-$ (**1c**), and $[Re(Cl_2\text{-}bdt)_3]^{1-}$ (**2c**) is derived from DFT calculations by using the B3LYP functional for geometry optimizations, the MO descriptions, and spin distributions in these complexes. Spin-unrestricted Kohn−Sham (UKS) DFT calculations were carried out with inclusion of scalar relativistic effects using the ZORA method. In general, the calculated geometries and metrical parameters of the complexes **1b**, **1c**, **2c**, and **3a**−**3e** presented in Table 7 were

(54) (a) Enderle, B.; Gates, B. C. *Phys. Chem. Chem. Phys.* **2004**, *6*, 2484. (b) Herro-Martín, J.; Subías, G.; Blasco, J.; García, J.; Sánche, M. C. *J. Phys.: Condens. Matter* **2005**, *17*, 4963. (c) Lukens, W. W.; McKeown, D. A.; Buechele, A. C.; Muller, I. S.; Shuh, D. K.; Pegg, I. L. *Chem. Mater.* **2007**, *19*, 559. (d) Nunes, C. D.; Pillinger, M.; Hazell, A.; Jepsen, J.; Santos, T. M.; Madureira, J.; Lopes, A. D.; Gonçalves, I. S. *Polyhedron* **2003**, *22*, 2799.

(55) (a) Dey, A.; Glaser, T.; Couture, M. M.-J.; Eltis, L. D.; Holm, R. H.; Hedman, B.; Hodgson, K. O.; Solomon, E. I. *J. Am. Chem. Soc.* **2004**, *126*, 8320. (b) Glaser, T.; Rose, K.; Shadle, S. E.; Hedman, B.; Hodgson, K. O.; Solomon, E. I. *J. Am. Chem. Soc.* **2001**, *123*, 442.

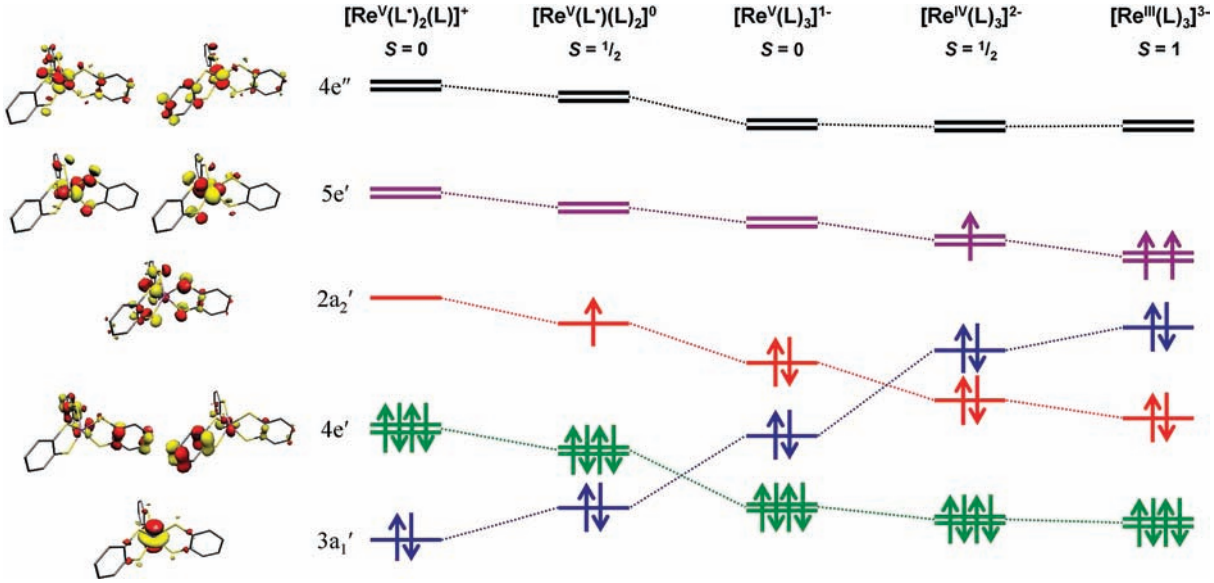

Figure 10. Qualitative MO scheme depicting the ordering of the frontier orbitals for the $[Re(L)_3]^z$ ($z = 1+, 0, 1-, 2-, 3-$) electron transfer series derived from B3LYP DFT calculations. The MOs shown on the left are derived from the $[Re(bdt)_3]^+$ calculation with D_{3h} symmetry labels.[56]

Table 7. Averaged Calculated Bond Distances (Å) and Angles (deg) Compared with Experimental Values in Parentheses

complex	1b	1c	2c	3a	3b	3c	3d	3e
Re−S	2.361	2.372(2.348)	2.365(2.340)	2.354	2.371	2.377	2.418	2.466
C−S	1.761	1.763(1.745)	1.757(1.743)	1.735	1.741	1.758	1.764	1.765
S−Re−S	81.9	80.9(81.0)	83.1(83.1)	83.7	82.7	82.7	83.0	82.9
Θ	0.37	0.02(0.46)	22.9(24.8)	0.05	0.34	24.9	33.5	41.4

found to be in very good agreement with experimental values where available, and moreover, the trend in the Re−S and intraligand bond distances is representative of the metal and ligand oxidation levels. While the mono-, di-, and trianions have structures ranging from distorted trigonal to near-octahedral, we will express their ground-state electron configurations in D_{3h} rather than D_3 symmetry, using the orbital terms coined originally by Gray et al.,[1] and Schrauzer and Mayweg[2] for a simple comparison of this electron transfer series.

Triplet State Trianion. A rhenium tris(dithiolene) trianion has only been observed by cyclic voltammetry, where at very negative potentials $[Re(bdt)_3]^{3-}$ (**3e**), $[Re(tdt)_3]^{3-}$,[1] and $[Re(Cl_4\text{-}bdt)_3]^{3-}$,[4] are generated. $[Re(bdt)_3]^{3-}$ was too unstable to be generated by controlled potential coulometry, and thus we have no experimental data to corroborate our calculations for this species. A UKS solution for the trianion, $[Re(bdt)_3]^{3-}$ (**3e**) was calculated using the B3LYP functional beginning with the coordinates from the optimized structure of the dianion (**3d**). The geometry optimized structure is near-octahedral with Θ = 41.4°, with long Re−S bonds at 2.466 Å (Table 7) and intraligand bond distances consistent with three closed-shell $(bdt)^{2-}$ ligands coordinated to a Re(III) d^4 central ion. This species carries a $(4e')^4(2a_2')^2(3a_1')^2(5e')^2$ electron configuration where the large twist angle results from populating the 5e′ MOs, which are antibonding with respect to a trigonal prism (Scheme S8, Supporting Information). The complex possesses D_3 symmetry with an $S = 1$ ground state, as exemplified by the Mulliken spin density plot (Figure S13, Supporting Information). The ordering of the principle orbitals defining the electronic structures of the five members of this electron transfer series are shown in Figure 10.

Doublet State Dianion. The calculated structure of the dianion $[Re(bdt)_3]^{2-}$ ($S = {}^1/_2$; **3d**) shows an absence of quinoidal distortion in the aromatic ring and long C−S bonds (av. 1.764 Å) consistent with three closed-shell $(bdt)^{2-}$ ligands coordinated to a Re(IV) (d^3) central ion. The geometry is less octahedral than the trianion (**3e**), with the twist angle calculated as Θ = 33.5°, similar to the angle witnessed in the only crystallographically characterized dianion, $[PPh_4]_2[Re(mnt)_3]$ (Θ = 38°).[42] The Re−S bonds are shortened to 2.419 Å compared to **3e**, consistent with a metal-centered oxidation. The dianion carries a $(4e')^4(2a_2')^2(3a_1')^2(5e')^1$ electron configuration (Figure 10) and is formulated as $[Re^{IV}(L)_3]^{2-}$. The Mulliken spin density plot (Figure 11a) shows one unpaired electron centered on Re, indicative of a low-spin Re^{IV} d^3 ion, in accord with its EPR spectrum. We have incrementally increased the twist angle (0−56°) for **3d** and performed a single point calculation at each step. The total energy was then plotted versus the twist angle, as shown in Figure 12. While there is an energy minimum at Θ = 30.4°, a trigonal prismatic structure is only 4.3 kcal mol^{-1} less stable (Figure 12).

Singlet State Monoanion. We have isolated three salts containing monoanions, two of which (**1c** and **2c**) are characterized crystallographically. Gratifyingly, the calculated Re−S, C−S, and $C_{arom}-C_{arom}$ bond lengths of **1c** and **2c** are in excellent agreement with the corresponding experimental values (Table 7); the difference in calculated and experimental values of C−S and $C_{arom}-C_{arom}$ bonds

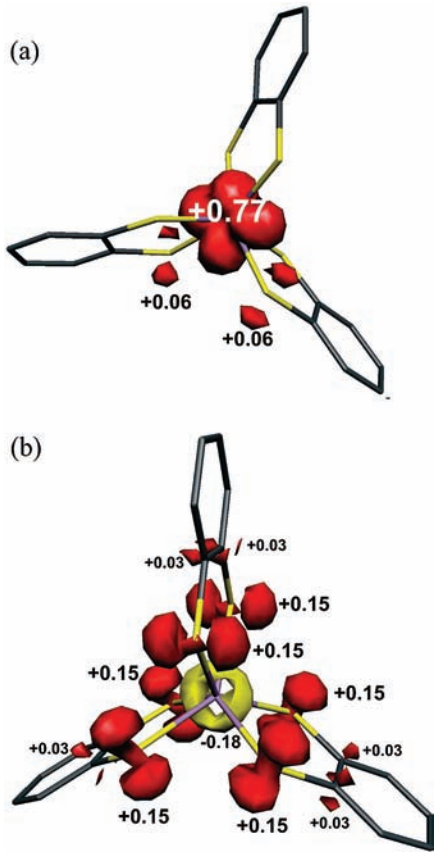

Figure 11. Spin density plots of (a) the dianion in **3d** and (b) neutral **3b**, from spin unrestricted DFT calculations together with values from the Mulliken analyses (red, α-spin; yellow, β-spin). A complete Mulliken spin density listing is available in the Supporting Information.

never exceeds 0.02 Å. The Re−S bond distances are overestimated by maximally 0.03 Å, which is a typical aspect of the B3LYP functional. The calculated av. C−S bond length of 1.763 Å in **1c** and 1.758 in **2c** (experimental av. C−S values of 1.745 and 1.743 Å, respectively) indicate the presence of closed-shell, dianionic dithiolate ligands as does the absence of quinoid-type distortions in the aromatic ring. The same observations hold for **3c**, where the calculations also indicate the presence of three $(bdt)^{2-}$ ligands. More interestingly, the calculated geometry of the monoanion in **1c** is trigonal prismatic; the average twist angle Θ is calculated to be 0.02° and observed (experimentally) at 0.46°. In contrast, the structure of **2c** is intermediate between trigonal prismatic and octahedral, with a calculated (and experimental) twist angle of 22.9° (24.8°). Both optimizations were initiated from the crystallographic coordinates. The calculated structure of $[Re(bdt)_3]^{1-}$ (**3c**) containing three *unsubstituted* benzene-1,2-dithiolate(2−) ligands is also distorted trigonal prismatic (Θ = 24.9°). Note that, with a decreasing number of $5d^n$ electrons (n = 4 in the trianion, 3 in the dianion, and 2 in the monoanion), the distortion of the near-octahedral ReS_6 polyhedron in **3e** to an intermediate structure in **3c** decreases, as is exemplified by the increasing calculated twist angle Θ, which is calculated to be 41.4° in **3e**, 33.5° in **3d**, and 24.9° in **3c**. Furthermore, the average calculated Re−S distances increase from 2.378 Å in **3c** to 2.419 Å in **3d** to 2.466 Å in **3e**. Thus, these structural parameters imply that the successive one-electron

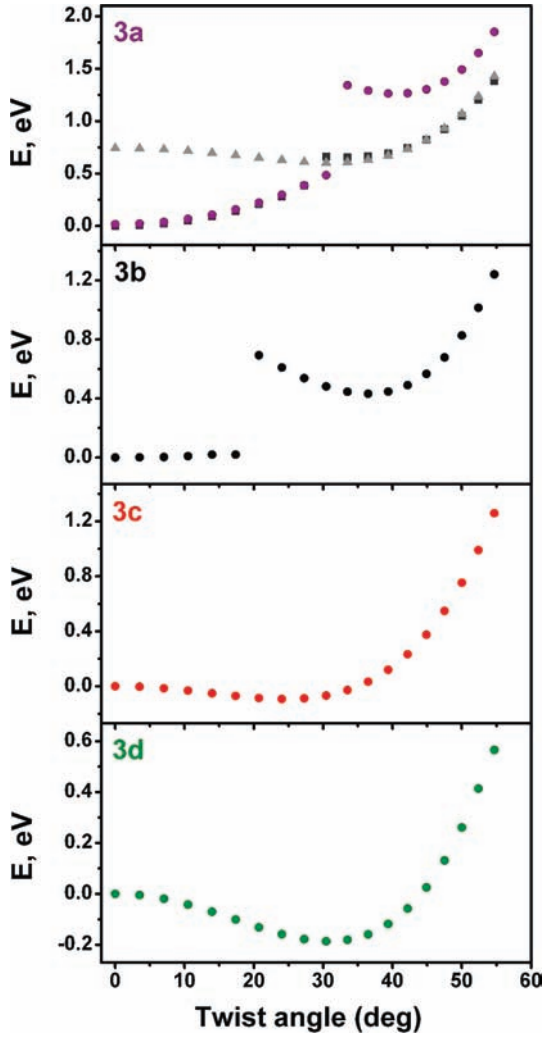

Figure 12. Walsh-type plot of the total electronic energies of **3a**−**3d** as a function of the trigonal twist angle (Θ). The relative total energy from the spin-unrestricted Kohn−Sham calculations for **3a**−**3d** is depicted by the filled circles. In each case, the energy for Θ = 0° has been set to zero. For **3a** (top), the total energy of the low-spin S=0 (squares) and high-spin S = 1 (triangles) solutions obtained from BS(1,1) DFT calculations are also shown.

oxidations of the tri- to the monoanion are metal-centered processes, as displayed in Figure 13. The Walsh-type plot for the incremental twisting of **3c**, as shown in Figure 12, identifies an energy minimum at Θ = 24° (the angle from optimization); however, most importantly, there is *only* a 2 kcal mol^{-1} difference in the total energy from 0° to 34°. A similar result has been obtained for **1c**, where the most energetically stable geometry is intermediate between a trigonal prism and an octahedron (25°) despite the crystallographic geometry being a perfect trigonal prism. It is important to note that the geometry did not relax at each specific twist angle (the bond distances and angle were fixed); however, we do obtain a trigonal prismatic structure when the optimization begins with trigonal prismatic coordinates (i.e., from the neutral molecule) and an intermediate structure when beginning with distorted octahedral coordinates (i.e., from the dianionic species). The energy difference between these two structures is very similar to the difference obtained from the single point calculations, underscoring

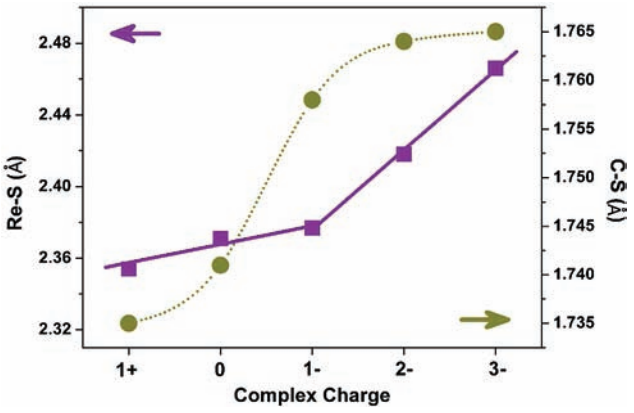

Figure 13. Plot of the av. calculated Re−S (squares) and av. C−S (circles) bond distances from the geometry optimization of **3a**−**3e** versus the complex charge. The two purple solid lines emphasize that reduction from **3a** to **3c** is ligand-centered, whereas **3c**−**3e** are linked by successive metal reduction. The spline curve (dotted line) highlights the shortening of the C−S bond distance when the $2a_2'$ MO is depopulated for neutral **3b** and monocationic **3a**.

the flat potential energy surface that encompasses a large range of twist angles. Therefore, in rhenium tris(dithiolene) monoanions, where the energy difference is <2.2 kcal mol^{-1} for twist angles ranging from 0 to 35°, crystal packing is highly influential in the observed crystallographic twist angles in **1c** and **2c**.

The qualitative MO scheme for **3c** displayed in Scheme S6 (see the Supporting Information) possesses the same MO ordering as that tendered by Al-Mowali and Porte,[5] though with twice as many orbitals owing to the different combinations of π orbitals from the aromatic ring. The highest occupied molecular orbital (HOMO) is the $2a_2$ orbital that is 100% ligand in composition. Populating this orbital should destabilize a trigonal prism because it increases the interligand repulsion since the phases of the sulfur 3p orbitals are antibonding with respect to each other. However, as seen both crystallographically and in the Walsh-type plot of **3c**, this is a very small energy value, which leads to the conclusion that the occupancy of this orbital has little bearing on the observed geometry. Beneath this is the $3a_1$ MO which has 31% Re d_{z^2} character. The a_1' and a_1'' orbitals in D_{3h} symmetry both transform as a_1 in D_3 symmetry (trigonal twisted) such that there are two MOs with ∼35% Re d_{z^2} character derived from the mixing of the purely $3a_1''$ ligand with the $3a_1'$ orbital comprising 70% d_{z^2}. This configurational interaction destabilizes the Re d_{z^2} orbital in these monoanionic species and has been recently implicated in producing different electronic grounds in molybdenum tris(dithiolene) monoanions.[11] However, the rhenium 5d orbital manifold is more stable than the Mo 4d manifold, and all of the monoanions possess a Re(V) d^2 central ion irrespective of the ligand substituents and complex geometry. The lowest unoccupied molecular orbitals (LUMOs) are degenerate combinations of the $d_{x^2-y^2,xy}$ and $d_{xz,yz}$ orbitals, and C−S π^* MOs. Overall, these monoanionic complexes have an electronic structure described as $[Re^{V}(L)_3]^{1-}$ ($S = 0$) with a $(4e')^4(3a_1')^2(2a_2')^2$ electronic configuration.

Doublet State Neutral Species. The optimized structure of neutral [Re(bdt)$_3$] ($S = {}^1/_2$) (**3b**) reveals a small shortening of the average C−S bond length to 1.741 Å and a small quinoid-type distortion of the benzene ring. This is classified as a ligand-centered oxidation where one-electron is removed from the $2a_2$ MO in **3c**, producing the neutral species **3b**. A similar scenario exists when **1c** is oxidized to **1b**. The changes in the average Re−S and C−S bond distances are charted in Figure 13, where oxidation of **3c** sees a pronounced shortening of the C−S bond length, whereas the Re−S bond length remains almost the same. Interestingly, the ReS_6 polyhedron in [Re(bdt)$_3$] is now calculated to be trigonal prismatic ($\Theta_{calcd} = 0.34°$), with a structure that closely resembles crystallographically characterized [Re(pdt)$_3$] containing three *cis*-1,2-diphenyl-1,2-dithiolene ligands.[3] Its electronic structure is defined as $[Re^{V}(L^{\bullet})(L)_2]^{0}$,[8] with the electron configuration of $(3a_1')^2(4e')^4(2a_2')^1$ (Figure 10) correctly issued by Al-Mowali and Porte.[5] The Mulliken spin plot displayed in Figure 11b shows that a small amount of spin density is found at the Re center ($\rho = -0.18$) through spin polarization of the Re−S π bonds of the 4e′ MOs. This generates the observed quadrupole-allowed transitions in the EPR spectrum of **3b**. The Walsh-type diagram for **3b** presented in Figure 12 shows $\Theta = 0°$ to be the most stable geometry. There is an abrupt increase in the total energy at $\Theta = 17.7°$ as twisting destabilizes the $3a_1'$ (now $3a_1$ in D_3 symmetry) orbital relative to the $2a_2'$ MO due to the aforementioned configurational interaction. Thus, the distorted octahedral structure has a $(4e')^4(2a_2')^2(3a_1')^1$ electron configuration, that is, a Re(VI) ion, originally proposed by Gray et al.[1] This second potential energy surface has a local minimum at $\Theta = 36.5°$ that is 10 kcal mol^{-1} higher in energy than the perfect trigonal prism, and recent calculations suggest this octahedral structure is a transition state.[57] We can geometry-optimize, starting from octahedral coordinates, and obtain distorted octahedral structure for **3b**. This species possesses a Re(VI) central ion, three dianionic dithiolate ligands, and a twist angle, $\Theta = 36.8°$. The energy of this structure is 8.2 kcal mol^{-1} higher than the trigonal prismatic solution and, reassuringly, is approximately the same energy as that of the single point molecule with the same twist angle.

Singlet-State Monocation. The monocation (**3a**) species of this series displays the shortest average C−S bonds at 1.725 Å and a longest $C_{arom}-C_{arom}$ distance of 1.424 Å and a significant quinoid-type distortion of the benzene ring, indicating a ligand-centered oxidation from **3b** to **3a** (Figure 13). The ReS_6 polyhedron remains trigonal prismatic ($\Theta_{calcd} = 0.05°$). With limited spectroscopic characterization of this complex, we must explore all plausible electronic structures that could give a trigonal prismatic solution, namely, $[Re^{V}(L^{\bullet})_2(L)]^{+}$, $[Re^{VI}(L^{\bullet})(L)_2]^{+}$, and $[Re^{VII}(L)_3]^{+}$. The Re(V) solution results from the UKS calculation, and, as shown in the Walsh-type diagram, is the most energetically favorable (Figure 12). Again, we observe an abrupt rise in the total energy at $\Theta = 31°$ where, at this angle, the configurational interaction (in D_3

(56) For consistency, D_{3h} symmetry labels are used to describe the electron configuration for all members of this electron transfer series despite the reduction in symmetry to D_3 when the molecule twists towards octahedral.

(57) Chandrasekaran, P.; Arumugam, K.; Jayarathne, U.; Pérez, L. M.; Mague, J. T.; Donahue, J. P. *Inorg. Chem.* **2008**, *48*, 2103.

symmetry) destabilizes the d_{z^2} orbital relative to the $2a_2'$ MO. This distorted octahedral structure from the UKS calculation (purple circles, Figure 12, top) is formulated as $[Re^{VII}(L)_3]^+$ and is 29.2 kcal mol^{-1} less stable than the trigonal prismatic solution. The $[Re^{VI}(L^{\bullet})(L)_2]^+$ electronic structure is a singlet diradical, with one unpaired electron on the Re ion and one hole in the dithiolene ligands. To investigate this, and the high-spin $M_S = 3$, we have used a broken symmetry BS(1,1) approach. As shown in Figure 12, the low-spin solution from the BS-(1,1) calculation converges to the $[Re^{V}(L^{\bullet})_2(L)]^+$ state found in the UKS calculation. This solution is 17.1 kcal mol^{-1} more stable than the high-spin ($S = 1$) state, when $\Theta = 0°$. At $\Theta > 33°$, there is a change to a new potential energy surface with a local minimum that lies 14 kcal mol^{-1} above the trigonal prismatic structure. This state carries a $(4e')^4(3a_1')^1(2a_2')^1$ electron configuration, where the $S = 0$ and $S = 1$ states are degenerate because the two SOMOs cannot mix in D_3 symmetry. Thus, we are confident that a one-electron oxidation of the neutral rhenium tris(dithiolene) is ligand-centered, producing a trigonal prismatic monocationic complex with a $(4e')^4(3a_1')^2(2a_2')^0$ electron configuration, wherein the depopulation of the $2a_2'$ MO gives rise to a more intense LLIVCT band, as seen in the electronic absorption spectrum of **1a**. This is an interesting molecule to study owing to the fact that it is isoelectronic to the neutral tris(dithiolene)molybdenum complexes. Recent XAS studies have produced two different electronic structures, either $[Mo^{IV}(mdt^{\bullet})_2(mdt)]$ or $[Mo^{V}(tbbdt^{\bullet})(tbbdt)_2]$,[11,13] where it appears that the redox potential of the ligand, which is reflected in the energy of the $2a_2'$ orbital with respect to the $4d_{z^2}$ ($3a_1'$), governs the oxidation state of the Mo ion. Most intriguingly, both complexes have very similar sulfur K-edge spectra,[11,13] which are difficult to justify with this apparent difference in the Mo oxidation state. Our calculation of the monocation shows, for the Re atom, that a d^2 system with two ligand holes is operative and is derived from the larger effective nuclear charge of Re that lowers the energy of the 5d orbitals, relative to the Mo 4d manifold. Molybdenum appears to be positioned at just the right energy that subtle changes in the π donor capabilities of the dithiolene ligand, through modifying the substituents, affects the ordering of the $3a_1'$ and $2a_2'$ orbitals such that we apparently have both Mo(IV) and Mo(V) centers in different neutral tris(dithiolene)molybdenum complexes. Importantly, the optimized structure of **3a** contains three very flat dithiolene ligands (av. $\alpha = 0.03°$) despite starting from the $[Mo(bdt)_3]$ crystal structure coordinates.[58] Dithiolene folding is present in all neutral tris(dithiolene) complexes of molybdenum[13,39,58,59] and the isoelectronic monoanionic vanadium compounds.[60] This is a second-order Jahn−Teller distortion whereby folding the dithiolene ligand facilitates HOMO−LUMO mixing through a $D_{3h} \rightarrow C_{3h}$ symmetry reduction that stabilizes the $3a_1'$ MO relative to the $2a_2'$ MO.[11,61]

h. Time-Dependent DFT Calculations. In order to obtain a deeper understanding of the pre-edge transitions in the S K-edge X-ray absorption spectroscopy, TD-DFT calculations have been used to assign the transitions seen in the S K-edge spectra of **1b** and **1c**. Additionally, these calculations also serve to calibrate the computed electronic structure with experimental results. Using a recently devised method for the calculation of K-pre-edge transitions,[34] we have simulated the S K-pre-edge region of **1b** and **1c** using the BP86 functional. For this system, there is a negligible difference in the electronic structure calculated by the BP86 and B3LYP functionals; hence, the former functional is preferred since it is considerably faster at computing the pre-edge. Additionally, due to the limitations in the accurate treatment of excited states in DFT, *absolute* transition energies cannot be obtained by this method. Nevertheless, the *relative* transition energies and the *relative* intensities are, in general, reliably modeled. For a given theoretical method, that is, combination of functional, basis sets, relativistic treatment, and so forth, an empirical correction for the energy and intensity can be introduced. For the present study, the calculated spectra are shifted by +61.45 eV.

The calculated S K-pre-edge spectra are shown in Figure 14 and afford an excellent fit of the experimental data. The peak energies and transition assignment are presented in Table 8. For the **1b**, two pre-edge peaks are calculated at 2470.09 and 2471.31 eV. The monoanion in **1c** has only one pre-edge feature calculated at 2471.05 eV. All of these values are within 0.12 eV of the experimental energies. It is significant that **1c** lacks the low-energy pre-edge transition found in **1b**, since this transition is characteristic of excitation to a hole in the S 3p orbitals. Here in trigonal prismatic geometry, it is defined as the $1s \rightarrow 2a_2'$ transition: one hole distributed over the three ligands. The second feature is assigned as the $1s \rightarrow 5e'$ transition, which is empty for both **1b** and **1c**, and thus has approximately the same intensity. The relative intensity of the two calculated pre-edge peaks for **1b** has exactly the same ratio (1.0:2.5) as the experiment. The second pre-edge peak is considerably broader experimentally (fwhm = 1.20 eV) than the first pre-edge peak (0.88 eV) and that used in the simulation (fixed at 0.8 eV).

Although there is no crystal structure for **1b**, the optimized Re−S bond distances do not vary by more than 0.017 Å. The only crystallographically defined rhenium tris(dithiolene) complex, $[Re(pdt)_3]$,[3] has six near-equivalent Re−S bond distances that implies that the three-fold axis is retained, and therefore, broadening of this band is not a consequence of nondegenerate $5e'$ MOs through a lowering of the symmetry. This broadening is caused by a small splitting of the spin-up (α-spin) and spin-down (β-spin) set of $5e'$ MOs by spin polarization rather than a reduction of the symmetry due to a molecular distortion. The TD-DFT calculates a splitting (between the $5e'(\alpha)$ and $5e'(\beta)$ orbitals)

(58) Cowie, M.; Bennett, M. J. *Inorg. Chem.* **1975**, *15*, 1584.

(59) (a) Friedle, S.; Partyka, D. V.; Bennett, M. V.; Holm, R. H. *Inorg. Chim. Acta* **2006**, *359*, 1427. (b) Smith, A. E.; Schrauzer, G. N.; Mayweg, V. P.; Heinrich, W. *J. Am. Chem. Soc.* **1965**, *87*, 5798. (c) Wang, K.; McConnachie, J. M.; Stiefel, E. I. *Inorg. Chem.* **1999**, *38*, 4334.

(60) (a) Livage, C.; Fourmigué, M.; Batail, P.; Canadell, E.; Coulon, C. *Bull. Soc. Chim. Fr.* **1993**, *130*, 761. (b) Broderick, W. E.; McGhee, E. M.; Godfrey, M. R.; Hoffman, B. M.; Ibers, J. A. *Inorg. Chem.* **1989**, *28*, 2902. (c) Welch, J. H.; Bereman, R. D.; Singh, P. *Inorg. Chem.* **1988**, *27*, 2862. (d) Chung, G.; Bereman, R.; Singh, P. *J. Coord. Chem.* **1994**, *33*, 331.

(61) Campbell, S.; Harris, S. *Inorg. Chem.* **1996**, *35*, 3285.

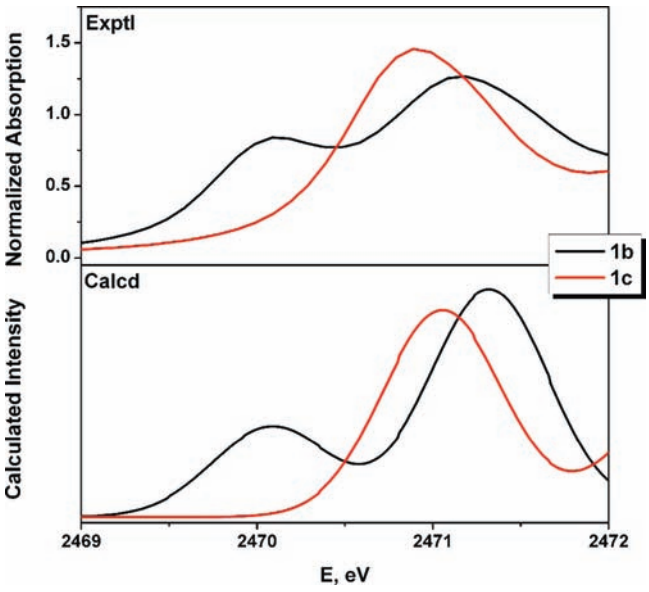

Figure 14. Experimental (top) and calculated (bottom) S K-edge XAS spectra of **1b** and **1c** obtained from BP86 TD-DFT calculations. Calculated intensity in arbitrary units.

Table 8. Comparison of Calculated and Experimentally Determined S K-edge XAS Spectra for **1b** and **1c**

		transition energies[a]		
	transition	exptl[b]	calcd[c]	area[b]
1b	$1s \rightarrow 2a_2'$	2470.05	2470.09	0.549
	$1s \rightarrow 5e'$	2471.20	2471.32	1.389
1c	$1s \rightarrow 5e'$	2470.94	2471.05	1.405

[a] In eV. [b] Derived from pseudo-Voigt deconvolution of the experimental spectrum. [c] Energy shifted +61.45 eV.

of 0.05 eV for **1b**, which is an underestimate of the experiment. The spin polarization in neutral rhenium tris(benzene-1,2-dithiolato) complexes is crucial in generating the large quadrupole coupling observed in the X-band EPR spectra. Diamagnetic **1c** has negligible spin polarization (equivalent $5e'(\alpha)$ and $5e'(\beta)$ orbitals) and has a sharper pre-edge peak (fwhm = 1.02 eV) that is of a similar width to the first pre-edge peak of **1b** (0.88 eV).

Conclusions

We have investigated each member of the electron transfer series [tris(benzene-1,2-dithiolene)rhenium]^z ($z = 1+, 0, 1-, 2-, 3-$) using a host of spectroscopies (UV−vis, EPR, XAS) and DFT calculations. Electrochemical measurements reveal that they are related by reversible one-electron transfer steps in solution. The most important result of this study is the fact that it is possible to unequivocally determine the spectroscopic oxidation state of the central rhenium ion (the $5d^n$ electron configuration) and the oxidation level of the dithiolene ligands.

It is clearly established that the diamagnetic monoanions $[Re(L)_3]^{1-}$ ($S = 0$) consist of three closed-shell dithiolato(2−) ligands and a central Re(V) ion (d^2, $S_{Re} = 0$). The structure of the ReS_6 polyhedron is (distorted) trigonal prismatic with twist angles Θ varying from 0.46° in **1c** to 24.8° in **2c**, as determined experimentally by X-ray crystallography and calculated by DFT. For **3c** containing unsubstituted benzene-1,2-dithiolate(2−) ligands, a twist angle of 24.9° has been calculated. The calculations show that the energetic profile for twist angles between 0° and ~34° is very shallow (within 2 kcal mol^{-1}) with packing forces being very influential on the observed twist angles. There is no clear electronic preference for an ideal trigonal prismatic versus a distorted trigonal prismatic structure.

The corresponding dianions $[Re(L)_3]^{2-}$ ($S = {}^1/_2$) consist again of three closed-shell benzene-1,2-dithiolate(2−) ligands and a low-spin central Re(IV) ion (d^3, $S_{Re} = {}^1/_2$). This is clearly shown by the X-band EPR spectrum that is dominated by the magnetic hyperfine of the Re nucleus. The calculated twist angle of 33.5° of the ReS_6 polyhedron indicates a geometry intermediate between trigonal prismatic and octahedral. Reduction of the dianion to the trianion $[Re(L)_3]^{3-}$ ($S = 1$) is again a metal-centered process yielding a central Re(III) ion (d^4, $S_{Re} = 1$) and three S,S'-coordinated dithiolate(2−) ligands. The ReS_6 polyhedron now approaches an octahedral geometry (Θ = 41.4°).

The most salient feature of this study is the observation that the neutral species $[Re(L)_3]$ ($S = {}^1/_2$) and the monocation $[Re(L)_3]^+$ ($S = 0$) contain both a trigonal prismatic ReS_6 polyhedron and a central low-spin Re(V) ion (d^2, $S_{Re} = 0$) with two electrons in the $5d_{z^2}$ metal orbital, namely, $(3a_1')^2$ in D_{3h} symmetry. The unpaired electron in neutral **3b** occupies a pure ligand MO, $(2a_2')^1$. This electron configuration is unequivocally confirmed by the EPR spectrum where a unique situation exists, in that the quadrupole interaction is larger than the magnetic hyperfine interaction. The electronic spectrum of **1b** and **3b** displays an intense ($> 10^4$ M^{-1} cm^{-1}) LLIVCT band at 684 and 674 nm, respectively, that is absent in the spectra of the mono-, di-, and trianions. The spectrum of **1a** shows this band at 661 nm. Thus, both the neutral and monocationic forms possess oxidized forms of the ligands (formally one and two ligand holes, respectively) and a central Re(V) ion. In the monocation, the ligand orbital $(2a_2')$ is empty (LUMO), whereas in the neutral form it is the SOMO and in the monoanion it is the HOMO (filled with two electrons). X-ray absorption spectroscopy at the S K edge and Re L edge provides direct spectroscopic evidence for the above interpretation. In summary, we have shown that the electronic structures of the five-membered electron transfer series $[Re(L)_3]^z$ ($z = 1+, 0, 1-, 2-, 3-$) is as follows: $[Re^V(L^\bullet)_2(L)]^+$, $[Re^V(L^\bullet)(L)_2]^0$, $[Re^V(L)_3]^{1-}$, $[Re^{IV}(L)_3]^{2-}$, $[Re^{III}(L)_3]^{3-}$.

Acknowledgment. This work is dedicated to Professor Wolfgang Lubitz on the occasion of his 60th birthday. We thank Dr. Eberhard Bothe and Ms. Petra Höfer for their technical expertise with electrochemical measurements. We are grateful for financial support from the Fonds der Chemischen Industrie. S.S. and F.L.B. thank the Max-Planck-Society for a postdoctoral fellowship and doctoral stipend, respectively. SSRL operations are funded by the Department of Energy, Office of Basic Energy Sciences. The Structural Molecular Biology program is supported by the National Institutes of Health (grant 5 P41 RR001209), National Center for Research Resources, Biomedical Technology Program and by the Department of Energy, Office of Biological Environmental Research.

Supporting Information Available: X-ray crystallographic files in CIF format for **1c** and **2c**. Cyclic voltammogram for **2c**; electronic absorption spectra of $[Re(Cl_2\text{-}bdt)_3]^z$ (z = 0, 1−, 2−); Re L_2-edge spectra of **1c**, **2c**, **3b**, **3c**, and **3d**; S K-edge spectra of **2c**, **3b**, and **3c**; and pseudo-Voigt fitting parameters for the S K-edge spectra of **1b** and **1c**. Tables of geometric and electronic structures details (qualitative MO schemes and Mulliken spin density plots) of DFT calculated structures of **1b**, **1c**, **2c**, and **3a**−**3e**. This material is available free of charge via the Internet at http://pubs.acs.org.